ARTICLE LINK: http://www.sciencedirect.com/science/article/pii/S0968090X15001266
PLEASE CITE THIS ARTICLE AS
Han, K., Sun, Y., Liu, H., Friesz, T.L., Yao, T., 2015. A bi-level model of dynamic traffic signal control with continuum approximation. Transportation Research Part C 55, 409-431.

A bi-level model of dynamic traffic signal control with continuum approximation

Ke Han[a,*], Yuqi Sun[b], Hongcheng Liu[b], Terry L. Friesz[b], Tao Yao[b]

[a]*Department of Civil and Environmental Engineering, Imperial College London, United Kingdom.*
[b]*Department of Industrial and Manufacturing Engineering, Pennsylvania State University, USA.*

Abstract

This paper proposes a bi-level model for traffic network signal control, which is formulated as a dynamic Stackelberg game and solved as a *mathematical program with equilibrium constraints* (MPEC). The lower-level problem is a *dynamic user equilibrium* (DUE) with embedded *dynamic network loading* (DNL) sub-problem based on the LWR model (Lighthill and Whitham, 1955; Richards, 1956). The upper-level decision variables are (time-varying) signal green splits with the objective of minimizing network-wide travel cost. Unlike most existing literature which mainly use an on-and-off (binary) representation of the signal controls, we employ a continuum signal model recently proposed and analyzed in Han et al. (2014), which aims at describing and predicting the aggregate behavior that exists at signalized intersections without relying on distinct signal phases. Advantages of this continuum signal model include fewer integer variables, less restrictive constraints on the time steps, and higher decision resolution. It simplifies the modeling representation of large-scale urban traffic networks with the benefit of improved computational efficiency in simulation or optimization. We present, for the LWR-based DNL model that explicitly captures vehicle spillback, an in-depth study on the implementation of the continuum signal model, as its approximation accuracy depends on a number of factors and may deteriorate greatly under certain conditions. The proposed MPEC is solved on two test networks with three metaheuristic methods. Parallel computing is employed to significantly accelerate the solution procedure.

Keywords: traffic signal control, dynamic Stackelberg game, dynamic user equilibrium, continuum signal model, vehicle spillback, mathematical program with equilibrium constraints

1. Introduction

Signalized intersections play a vital role in the design, management and control of urban traffic networks. These locations are often very important restrictive bottlenecks, and therefore urban traffic control strategies tend to focus on the operation of signalized intersections (Miller, 1963; Robertson and Bretherton, 1974; Shelby, 2004; Guler and Cassidy, 2012; Gayah and Daganzo, 2012).

There are multiple approaches of designing and optimizing traffic signal controls on a road network, among which we distinguish between heuristic methods, such as feedback control, genetic algorithms and fuzzy logic; and exact approaches such as mathematical programming and optimal control. Cao et al (1999) apply fuzzy logic methods to

*Corresponding author
Email addresses: k.han@imperial.ac.uk (Ke Han), yuqisun19@gmail.com (Yuqi Sun), hql5143@psu.edu (Hongcheng Liu), tfriesz@psu.edu (Terry L. Friesz), tyy1@engr.psu.edu (Tao Yao)

determine useful junction control rules in a dynamic environment. Lin et al (1997) provide a framework for implementing adaptive traffic signal controllers based on fuzzy logic. In another line of research, Improta and Cantarella (1984) formulate a traffic signal control problem at a single road junction as a mixed integer program (MIP). Lo (1999a) and Lo (1999b) employ the cell transmission model (Daganzo, 1994, 1995) to formulate a signal control problem as an MIP . Han et al. (2014) further reduce the number of binary variables and eliminate the vehicle holding problem in the MIP by applying the link transmission model (Yperman et al., 2005). These optimization problems reviewed above are viewed as single-level problems as they treat traffic load at the signalized network as exogenous and do not address drivers' reactions to the implemented signal timings in terms of their route or departure time choices.

On the other hand, signal optimization problems that address drivers' adaptive travel choices as a result of the change in signal timings tend to exhibit a bi-level structure. On the lower level, road users are modeled as non-cooperative Nash players who selfishly minimize their own travel costs by adjusting departure time and/or route choices. On the upper level, a central planner seeks to maximize the network performance through a carefully designed signal plan, which is informed by the prediction of the behavior of the lower-level players (drivers). This bi-level problem is expressed as a *Stackelberg game* and formulated as a *mathematical program with equilibrium constraints* (MPEC).

In a bi-level decision-making environment, the influence of signal timing on route choices is first addressed by Allsop (1974), who considers signal decisions in the presence of a static user equilibrium. Yang and Yagar (1995) apply a sensitivity analysis based on Friesz et al. (1990) to determine the derivatives of link flow and delay in the equilibrium state of a bi-level problem. The above work is extended by Cantarella et al. (1991) and Cantarella et al. (1995), who take into consideration signal settings including cycle length, offset and green split. They derive a lower normative bound and an upper descriptive bound for the solution of signal settings in a traffic network under equilibrium flow. Meneguzzer (1995) develops a route choice user equilibrium (UE) model that incorporates intersection operations with flow-responsive traffic signals. Machemehl and Lee (2005) develop a variety of algorithms such as genetic algorithm, local search optimization and assignment methods to solve an optimal combined UE and signal control problem. Most of the aforementioned studies consider static traffic assignment models and static signal strategies.

In the venue of dynamic traffic modeling and optimization, Abdelfatah and Mahmassani (1998) and Abdelfatah and Mahmassani (2001) consider dynamic traffic signal models and propose a simulation-based solution approach. Gartner and Stamatiadis (1998) present an intelligent transportation system that incorporates both a dynamic traffic assignment module for traffic prediction and a real-time adaptive traffic control system. Chen and Ben-Akiva (1998) consider the combined dynamic user equilibrium (DUE) and signal control problem as a non-cooperative game between traffic controller and road users, which is solved using game-theoretic techniques. Sun et al. (2006) employ a heuristic solution approach for dynamic traffic signal optimization in networks with time-dependent demands and stochastic route choices. The lower level problem in their paper is a *reactive dynamic user optimal* problem, as opposed to the so-called *predictive dynamic user equilibrium* (Friesz et al., 1993). Karoonsoontawong and Waller (2009) propose a mixed-zero-one continuous linear bi-level formulation of the combined dynamic user optimal and traffic signal optimization problem. However, their problem solution is chosen among some pre-defined signal timing plans. Ukkusuri et al. (2013) formulate a signal optimization problem as a game between signal operator and road users. They solve a problem with time-varying signal cycle and split on a small test network with an iterative optimization-and-assignment method. In all the aforementioned dynamic traffic signal control models and methods, the signal controls are captured by binary variables.

This paper presents a bi-level differential Stackelberg game formulation of the network signal control problems with special attention given to the modeling of signalized intersections in the *dynamic network loading* (DNL) subproblem. In particular, unlike the previously reviewed papers, which all consider the on-and-off (binary) representation of signal controls, we employ the Lighthill-Whitham-Richards (LWR) (Lighthill and Whitham, 1955; Richards, 1956) model integrated with a *continuum signal model* (Han et al., 2014), which does not rely on distinct signal phases. In the continuum signal model, a fraction, η, of the downstream links' capacity is assumed to be available to vehicles discharged from a given approach during the entire signal cycle. η is assumed to be equal to the green proportion of the cycle allocated to the subject approach for movement through the intersection. The continuum signal model has a number of distinctive advantages over its on-and-off counterpart: (1) it requires fewer integer variables when modeling dynamics on large-scale networks, which reduces the computational complexity of the modeling and optimization processes; (2) it provides more flexibility in selecting the time step size and thus increases the computational

efficiency; (3) it eliminates discontinuities in path travel times that naturally arise from an on-and-off signal representation, which allows DUE problems to be formulated in a more exact way without the need to introduce user bounded rationality (Szeto and Lo, 2006; Ge and Zhou, 2012; Han et al., 2014); and (4) it allows higher decision resolution in terms of the green time allocated to each approach. The continuum signal model is suitable for predicting the aggregate behavior that exists in large-scale signalized networks without having to handle the detailed and random signal sequences at local intersections. When appropriately utilized, the continuum model can accurately predict the average throughput of traffic bottlenecks, and capture the effect of queue spillbacks.

Nevertheless, as pointed out by Han et al. (2014) through theoretical investigation of the model, the accuracy of the continuum model as an approximation of the on-and-off model is affected by a number of factors, including the fundamental diagram and whether or not spillback is present. Such a complication arises from potential vehicle spillbacks that are captured by the LWR-based DNL model. Following the insights provided by Han et al. (2014), we propose in this paper a DNL procedure that incorporates the continuum signal model and maximizes its approximation efficacy. A numerical case study is provided in Section 3.4 to illustrate the effectiveness of this DNL procedure.

The lower-level problem is formulated as a simultaneous route-and-departure-time choice dynamic user equilibrium (Friesz et al., 1993, 2011, 2013), with the LWR-based DNL sub-problem that incorporates the continuum signal model. The upper-level problem, as we have previously mentioned, is formulated as an MPEC problem. We make note of the fact that this MPEC is computationally challenging and does not admit analytical and exact solution schemes due to the fact that the control variables (signal green splits) are embedded in the LWR-based DNL procedure, which is known to have poor regularities (due to shock waves and complex junction models) and cannot be differentiated in any weak sense. Adding even more computational difficulty to the problem is the fact that the proposed MPEC is highly non-convex and has a semi-infinite constraint due to the variational inequality formulation of DUE (Friesz et al., 1993). With these difficulties in mind, we solve the proposed MPEC problem using three different metaheuristic methods: *simulated annealing*, *particle swarm optimization*, and *nested partition*. These metaheuristics do not assume any knowledge beyond the zeroth-order information on the objective function and constraints, and thus are suitable for optimization problems in which gradients or second-order information are unknown or difficult to calculate. Moreover, although they enjoy less rigorous results regarding convergence, solution quality and overall performance, they provide a more flexible trade-off between computational overhead and solution quality and often yield good solutions with reasonable computational costs. An introduction to these metaheuristic methods and a more elaborated discussion of their advantages are provided in Section 4. These metaheuristics are performed for networks with small and medium sizes, and implemented on a parallel computing platform to accelerate their solution procedures. In summary, contributions made in this paper are listed below.

- We propose a bi-level, dynamic Stackelberg game formulation for the design of network signal timing, which is able to capture drivers' adaptive travel choices and their reactions to signal timings. The embedded DNL procedure employs the LWR model that captures vehicle spillback, and the continuum signal junction model which has a few considerable advantages over its on-and-off counterpart.

- We show, through a detailed analysis of vehicle spillback, how the approximation efficacy of the continuum signal model depends on (1) the fundamental diagram; and (2) the presence of queue spillback. Further interpretation of the approximation error and modeling suggestions are provided.

- We propose three metaheuristic methods for solving the MPEC problem. These methods are described in detail and compared with each other in terms of solution quality and computational efficiency. A parallelization of one of the metaheuristics is also presented.

Notice that our proposed optimization problem does not concern the cycle length or the signal phasing schemes as they are not explicitly considered by the continuum signal models; moreover, we are focusing on the aggregate intersection throughputs in large signalized networks rather than detailed vehicle movements at a granular level. The signal cycles and phases may be determined separately or in conjunction with our optimized green splits to maximize intersection capacity and safety.

The rest of this paper is organized as follows. Section 2 presents some essential background of dynamic user equilibrium, including its formulation and solution algorithm. Section 3 provides a comprehensive assessment of the continuum signal model in a dynamic network loading procedure, following the theoretical guidance from Han et al.

(2014). In Section 4, the MPEC formulation is presented, followed by detailed description of the three metaheurstic solution methods. Section 5 presents several numerical examples. Finally, Section 6 offers some concluding remarks.

2. The dynamic user equilibrium as the lower-level problem

As the lower-level problem of the proposed bi-level formulation, the dynamic user equilibrium (DUE) considered in this paper captures two aspects of driving behavior: departure time choice and route choice (Friesz et al., 1993). Within the DUE model, *experienced* travel cost, including travel time and early/late arrival penalties, is identical for those route and departure time choices selected by travelers between a given origin-destination (O-D) pair.

In the last two decades there have been many efforts to develop a theoretically sound formulation of dynamic network user equilibrium that is also a canonical form acceptable to scholars and practitioners alike. As pointed out by Han (2013), there are two essential components within the notion of DUE: (i) the mathematical expression of Nash-like equilibrium conditions, and (ii) a network performance model, which is, in effect, an embedded dynamic network loading (DNL) problem. There are multiple means of expressing the Nash-like notion of a dynamic equilibrium mathematically, including a variational inequality (Friesz et al., 1993; Smith and Wisten, 1994, 1995), an evolutionary dynamic (Mounce, 2006; Smith and Wisten, 1995), a nonlinear complementarity problem (Wie et al., 2002; Han et al., 2011), a differential variational inequality (Friesz et al., 2011, 2013; Friesz and Mookherjee, 2006), and a differential complementarity system (Pang et al., 2011). Clearly, another key component of the DUE is the path delay operator, typically obtained from dynamic network loading (DNL), which is a sub-problem of a complete DUE model. The DNL captures the relationships among arc entry flow, arc exit flow, arc delay and path delay for any set of path departure rates. Any DNL must be consistent with the established path departure rates and link delay model, and it is usually performed under the *first-in-first-out* (FIFO) rule. Examples of some commonly employed link performance models include the *M-N* model (Merchant and Nemhauser, 1978a,b), the *link delay model* (Friesz et al., 1993), the *Vickrey model* (Vickrey, 1969; Han et al., 2013a,b), the LWR-Lax model (Bressan and Han, 2011, 2012; Friesz et al., 2013), the *cell transmission model* (Daganzo, 1994, 1995), and the *link transmission model* (Yperman et al., 2005).

2.1. Formulation and algorithm of the DUE problem

We consider a fixed time horizon $[t_0,\, t_f] \subset \mathbb{R}$ where $\mathbb{R}$ denotes the set of real numbers [1]. The most crucial component of the DUE model is the path delay operator which, given a set of path departure rates, provides the time needed to traverse any path p with any given departure time. The path delay is denoted by

$$D_p(t,\, h) \qquad \forall\, p \in \mathcal{P}, \quad \forall\, t \in [t_0,\, t_f]$$

where $\mathcal{P}$ is the set of paths employed by travelers, t denotes the departure time, and h is a vector of departure rates. We stipulate that each path departure rate $h_p(\cdot)$, as a function of departure time t, is non-negative and square-integrable, and thus belong to the set $L^2_+[t_0,\, t_f]$ where $L^2[t_0,\, t_f]$ is the space of square-integrable functions defined on the interval $[t_0,\, t_f]$, and the subscript '+' indicates non-negativity. For the complete vector of path departure rates $h(\cdot) = (h_p(\cdot) : p \in \mathcal{P})$, we have that $h \in (L^2_+[t_0,\, t_f])^{|\mathcal{P}|}$ where $(L^2[t_0,\, t_f])^{|\mathcal{P}|}$ is the $|\mathcal{P}|$-fold product of the space $L^2[t_0,\, t_f]$.

The path delay (path travel time) is combined with an arrival penalty to form the more general notion of travel cost:

$$\Psi_p(t,\, h) \;\doteq\; D_p(t,\, h) + \mathcal{F}\Big(t + D_p(t,\, h) - T_A\Big) \tag{2.1}$$

where $\mathcal{F}(\cdot)$ is the penalty function for early or late arrival relative to the target arrival time T_A. Note that, for convenience, T_A is assumed to be independent of the O-D pair. However, that assumption is easy to relax, and the consequent generalization of our model is a trivial extension. We interpret $\Psi_p(t,\, h)$ as the perceived travel cost of driver departing at time t along path p, when the collective travel decisions of all drivers are encapsulated by the path departure rate vector h.

[1] In subsequent presentation we will use $\mathbb{R}_+$ and $\mathbb{R}_{++}$ to denote the set of non-negative and positive real numbers, respectively.

To support the development of a dynamic network user equilibrium model, we introduce some additional constraints. Foremost among these are the flow conservation constraints, also known as the demand satisfaction constraints:

$$\sum_{p\in\mathcal{P}_{ij}} \int_{t_0}^{t_f} h_p(t)\,dt \;=\; Q_{ij} \qquad \forall\,(i,\,j)\in\mathcal{W} \tag{2.2}$$

where $\mathcal{P}_{ij}$ is the set of paths connecting the O-D pair $(i,\,j)\in\mathcal{W}$, and $\mathcal{W}$ is the set of all O-D pairs in the network. In addition, Q_{ij} is the fixed travel demand for O-D pair $(i,\,j)$. Using the notation and concepts we have thus far introduced, the set of feasible solutions for the DUE problem is

$$\Lambda \;=\; \left\{ h\in\left(L^2_+[t_0,\,t_f]\right)^{|\mathcal{P}|} :\quad \sum_{p\in\mathcal{P}_{ij}} \int_{t_0}^{t_f} h_p(t)\,dt \;=\; Q_{ij} \quad \forall\,(i,\,j)\in\mathcal{W} \right\} \tag{2.3}$$

Using a presentation very similar to the above, the notion of a dynamic user equilibrium in continuous time is first introduced by Friesz et al. (1993), who employ a definition tantamount to the following:

Definition 2.1. ***(Dynamic user equilibrium)*** *A vector of departure rates $h^*\in\Lambda$ is a dynamic user equilibrium if*

$$h^*_p(t) > 0, p\in\mathcal{P}_{ij} \Longrightarrow \Psi_p(t,\,h^*) = v_{ij}\in\mathbb{R}_{++} \quad \forall(i,\,j)\in\mathcal{W} \tag{2.4}$$

where v_{ij} denotes the minimum travel cost within the O-D pair $(i,\,j)$ for all path and departure time choices. We denote the dynamic user equilibrium defined this way by $DUE(\Psi,\Lambda,\,[t_0,\,t_f])$.

In the analysis to follow, we focus on the following variational inequality formulation of the DUE problem reported in Theorem 2 of Friesz et al. (1993).

$$\left.\begin{array}{c} \text{find } h^*\in\Lambda \text{ such that} \\ \sum\limits_{p\in\mathcal{P}} \int\limits_{t_0}^{t_f} \Psi_p(t,h^*)(h_p(t)-h^*_p(t))dt \;\geq\; 0 \\ \forall h\in\Lambda \end{array}\right\} VI(\Psi,\,\Lambda,\,[t_0,\,t_f]) \tag{2.5}$$

The variational inequality formulation $VI(\Psi,\,\Lambda,[t_0,\,t_f])$ expressed above subsumes almost all DUE models regardless of the arc dynamics or the network loading models employed.

Computational methods for DUEs vary, depending on the specific mathematical formulation used to express the problem. In this paper we provide a fixed-point algorithm based on the *differential variational inequality* (DVI) formulation (Friesz et al., 2011). The relationship between the DVI formalism and the DUE is revealed by expressing the VI as a fictitious optimal control problem and then applying the minimum principle. Furthermore, the fixed-point algorithm is derived in a similar fashion by solving a linear-quadratic optimal control problem. The reader is referred to Friesz et al. (2013) for a detailed discussion on the DVI and the fixed-point method.

Fixed-point method

Step 0 Identify an initial feasible point $h^0\in\Lambda$. Set the iteration counter $k=0$. Let $\alpha>0$ be a fixed constant.

Step 1 Solve the dynamic network loading sub-problem with path departure rates given by h^k, and obtain the path travel cost $\Psi_p(t,\,h^k),\ \forall p\in\mathcal{P},\ \forall t\in[t_0,\,t_f]$.

Step 2 For each $(i,\,j)\in\mathcal{W}$, solve the following algebraic equation for μ_{ij}, using root-search algorithms.

$$\sum_{p\in\mathcal{P}_{ij}} \int_{t_0}^{t_f} \left[h^k_p(t) - \alpha\Psi_p(t,\,h^k) + \mu_{ij}\right]_+ dt \;=\; Q_{ij}$$

Then update the next iterate $h^{k+1}(\cdot) = \{h^{k+1}_p(\cdot) : p\in\mathcal{P}\}$ where

$$h^{k+1}_p(t) \;=\; \left[h^k_p(t) - \alpha\Psi_p(t,\,h^k) + \mu_{ij}\right]_+ \qquad \forall p\in\mathcal{P}_{ij},\ \ (i,\,j)\in\mathcal{W}$$

where $[x]_+ \doteq \max\{0,\,x\}$.

Step 3 Terminate the algorithm with output $h^* \approx h^k$ if

$$\left\|h^{k+1} - h^k\right\|_{L^2} \Big/ \left\|h^k\right\|_{L^2} \;\leq\; \epsilon$$

where $\epsilon \in \mathbb{R}_{++}$ is a prescribed termination threshold, and the norm $\|\cdot\|_{L^2}$ is defined as

$$\|h\|_{L^2} \;=\; \left(\sum_{p\in\mathcal{P}} \int_{t_0}^{t_f} \left(h_p(t)\right)^2 dt\right)^{1/2}$$

Otherwise, set $k = k + 1$ and repeat Step 1 through Step 3.

3. Continuum modeling of signalized intersections in the dynamic network loading sub-problem

This section focuses on the dynamic network loading sub-problem of DUE; that is, Step 1 of the fixed-point algorithm presented above. The embedded network loading problem captures the relationships among arc entry flows, arc exit flows, arc delays and path delays for any given set of path departure rates, in connection with exogenous network configurations or controls such as traffic signal timings, as we consider in this paper.

A central focus of this section and also of this paper is to incorporate in the DNL procedure a signal control mechanism , which not only describes the aggregate behavior that exists at signalized intersections in large urban networks, but also facilitates efficient computation of the DNL sub-problem. For reasons well stated in the introductory part of this paper, we consider the continuum signal model (Han et al., 2014) as an alternative representation of the binary signal controls. Notably, as pointed out by Han et al. (2014), application of the continuum model is less straightforward than it appears: the error of the continuum approximation is dependent not only on the fundamental diagram employed by the LWR model but also on whether or not spillback occurs in the traffic network of interest. The main purpose of this section is to illustrate these modeling subtleties and make recommendations regarding the use of the continuum signal model. In order to provide a comprehensive introduction to relevant signal models and to be self-contained, we provide within this section some definitions and terminologies required to describe the exact on-off signal model and the continuum signal model.

3.1. Problem setup and terminology

Given a fixed time horizon $[0, T]$, and any link I_i in the network where $i = 1, 2, \ldots$, we define its signal control to be a binary and periodic function $u_i(\cdot) : [0, T] \to \{0, 1\}$ such that $u_i(t)$ equals one if the subject approach receives the green signal, and zero if it receives the red signal. The cycle length, denoted Δ_i, is equal to the period of $u_i(\cdot)$. A split parameter $\eta_i \in (0, 1)$ is used to describe the green time allocated to the link I_i; therefore, the actual green time provided to link I_i is $\eta_i\Delta_i$ in a full cycle.

We next turn to link-specific parameters. It is assumed throughout this paper that the fundamental diagrams that describe traffic on all links satisfy the following mild assumptions:

(F) The fundamental diagram is concave, continuous, and vanishes at $\rho = 0$ and $\rho = \rho^{jam}$.

where ρ denotes vehicle density, and ρ^{jam} denotes jam density. We also let ρ^c be the unique critical density at which flow is maximized, C be the flow capacity, and L be the link length. All these parameters naturally vary from link to link, and we will always stick to the convention of using subscript 'i' to indicate their dependence on link I_i, $i = 1, 2, \ldots$.

Each link I_i is expressed as a spatial interval $[a_i, b_i] \subset \mathbb{R}$. The density is denoted $\rho_i(t, x)$, for $(t, x) \in [0, T] \times [a_i, b_i]$. The *demand* $D_i(t)$ and *supply* $S_i(t)$ of this link are defined according to Lebacque and Khoshyaran (1999) as:

$$D_i(t) = \begin{cases} C_i & \text{if } \rho_i(t, b_i-) \geq \rho_i^c \\ f_i(\rho_i(t, b_i-)) & \text{if } \rho_i(t, b_i-) < \rho_i^c \end{cases} \qquad S_i(t) = \begin{cases} C_i & \text{if } \rho_i(t, a_i+) < \rho_i^c \\ f_i(\rho_i(t, a_i+)) & \text{if } \rho_i(t, a_i+) \geq \rho_i^c \end{cases} \tag{3.6}$$

The notion of *effective supply* is of crucial importance to the definition of signal models.

Definition 3.1. (Effective supply) *Given any link I_i, the effective supply for this link, denoted by $\mathcal{E}_i(t)$, is defined as follows. Let $\{I_j : j = 1, 2, \ldots, m_i\}$ be the set of downstream links of I_i. For each downstream link I_j, define the car turning percentage $\alpha_{i,j}(t) \geq 0$ such that $\sum_{j=1}^{m_i} \alpha_{i,j}(t) \equiv 1$ for all t. Then*

$$\mathcal{E}_i(t) \doteq \min\left\{C_i\,,\ \min_{j=1,\ldots,m_i}\left\{\frac{S_j(t)}{\alpha_{i,j}(t)}\right\}\right\} \tag{3.7}$$

The time-varying quantity $\mathcal{E}_i(t)$ expresses the downstream capacity available for I_i when it receives the green light.

3.2. Definition of the on-and-off and continuum signal models

This section provides a brief review of the on-and-off and continuum signal models proposed and analyzed in Han et al. (2014). Throughout this paper we will adopt the naming convention of using the superscripts 'Δ' and '0' to represent quantities associated with the on-and-off signal model and the continuum signal model, respectively. Using the signal control $u_i(t)$ and effective supply $\mathcal{E}_i(t)$ for link I_i, the on-and-off model for this link is expressed in terms of its downstream boundary condition as:

$$f^{\Delta}_{out,i}(t) = \min\left\{D_i(t),\ u_i(t)\mathcal{E}_i(t)\right\} \qquad \text{(On-and-off signal model)} \tag{3.8}$$

where $f^{\Delta}_{out,i}(t)$ denotes the exit flow of I_i. On the other hand, the continuum signal model is defined as:

$$f^{0}_{out,i}(t) = \min\left\{D_i(t),\ \eta_i\mathcal{E}_i(t)\right\} \qquad \text{(Continuum signal model)} \tag{3.9}$$

Remark 3.2. *The difference between the on-and-off model and the continuum model lies in the way downstream boundary conditions are specified. A general network flow problem also involves initial and upstream boundary conditions, which are implicitly considered here. In other words, the results concerning the continuum model presented below will hold with any given initial and upstream boundary conditions. The reader is referred to Han et al. (2014) for a Lax-Hopf treatment of various conditions in conjunction with the Hamilton-Jacobi equation and the Moskowitz function (Moskowitz, 1965).*

It should be noted that we assume here, as in nearly all first-order traffic flow models, that vehicles accelerate and decelerate instantaneously. Of course, acceleration rates are bounded in reality, and this complication will introduce an additional source of error. In practice, this is usually accounted for by including lost times at the signal where flow is zero, and modeling saturation flows during the effective green time. The methodological framework presented in this paper can be easily modified to incorporate the inclusion of lost times and/or yellow times: simply relax the assumption that the sum of the priority parameters is equal to one and instead let this sum be equal to the fraction of the cycle during which vehicles are allowed to discharge at saturation. This fraction can usually be detrained fairly easily in practice for a given cycle length.

3.3. Approximation efficacy of the continuum signal model

The continuum signal model enjoys some modeling and computational advantages as stated in Section 1. However, its accuracy in approximating the on-and-off signal model in a dynamic network where spillback is likely to occur is conditional. In a recent work (Han et al., 2014), the authors conduct rigorous analyses on the approximation error of the continuum signal model under a number of network conditions involving no spillback, sustained spillback, and transient spillback, to be defined and elaborated below. In order to be self-contained, we repeat in this section some key findings made by Han et al. (2014).

We start by noting that, by applying the continuum signal model instead of the on-and-off model, one is expected to observe quite different density profiles such as shock waves, rarefaction waves, and boundary conditions associated with the LWR conservation law. In other words, the continuum signal model in general overlooks detailed queuing and discharging of vehicles, and yields very different profiles of flow, density, or velocity compared to the on-and-off model. However, the continuum model is meant to describe the aggregate traffic behavior and throughput at signalized intersections, an indicator of which is the cumulative vehicle count. This observation leads us to the Hamilton-Jacobi equation and its solutions (cumulative vehicle counts). More precisely, we introduce the Moskowitz function $N(t, x)$,

which measures the cumulative number of vehicles that have passed location x by time t. The function $N(t,\ x)$ satisfies the following Hamilton-Jacobi equation

$$\partial_t N(t,\ x) - f(\ -\partial_x N(t,\ x))\ =\ 0 \qquad (t,\ x) \in [0,\ T] \times [a,\ b] \tag{3.10}$$

subject to initial condition, upstream and downstream boundary conditions. The analysis of the signalized junction involves a semi-analytical solution representation of the Hamilton-Jacobi equation (3.10), namely the generalized Lax-Hopf formula (Aubin et al., 2008; Claudel and Bayen, 2010). For the compactness of our presentation we only show relevant results below, and refer the reader to Han et al. (2014) for more detailed discussion and proof.

3.3.1. The case without spillback

Without loss of generality, we focus on the signalized junction A shown in Figure 1. Under the assumption that no spillback occurs at A, Han et al. (2014) show that the continuum model approximates well the Moskowitz functions on all the relevant links. Specifically, it is proven that the continuum approximation error is bounded uniformly and does not grow with time. Theorem 3.3 below is a precise statement. Notice that although these results are stated for link I_1, it is straightforward to re-state those results for link I_2, and more generally, for more complex junction topology and movements.

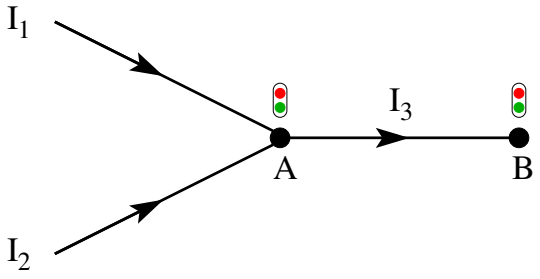

Figure 1: A signalized merge junction.

Theorem 3.3. (Han et al., 2014) *Consider the merge junction A depicted in Figure 1, and a signal control $u_1(t)$ for link I_1 with cycle Δ_A and green split $\eta_1 \in (0,\ 1)$. Given the same initial and upstream boundary conditions for I_1, let $N_1^{\Delta_A}(t,\ x)$ and $N_1^0(t,\ x)$ be the solutions of the H-J equation on I_1 with the additional downstream boundary condition specified by* (3.8) *and* (3.9) *respectively. Furthermore, assume that the entrance of link I_3 remains in the uncongested phase. Then, we have*

$$\left|N_1^{\Delta_A}(t,\ x) - N_1^0(t,\ x)\right|\ \le\ \eta_1(1-\eta_1)\Delta_A \min\{C_1, C_3\}\ \le\ \frac{1}{4}\Delta_A \min\{C_1, C_3\} \tag{3.11}$$

In particular, $N_1^{\Delta_A}(t,\ x) \to N_1^0(t,\ x)$ uniformly for all $(t,\ x) \in [0,\ T] \times [a_1,\ b_1]$, as $\Delta_A \to 0$.

3.3.2. The case with sustained spillback

When spillback occurs at junction A and persists for a certain amount of time (no less than a full cycle), for which we call the *sustained spillback*, the approximation accuracy of the proposed continuum model may be compromised In fact, the aforementioned error estimate and convergence does not hold if the fundamental diagram is triangular, and the error may grow with time and become unbounded. This will be illustrated using the following example.

Consider again the merge junction in Figure 1. Let us focus on I_3 which remains in the congested phase. In the spatial-temporal domain of I_3, characteristic lines with slope $-w_3$, which represent kinematic waves, emit from the downstream boundary $x = b_3$ and reach the upstream boundary $x = a_3$, where w_3 denotes the backward wave speed (see Figure 2). When the light is red, the exit flow $q_{out,3}$ is equal to zero, creating a kinematic wave with speed $-w_3$ and density value ρ_3^{jam}; when the light is green, the exit flow $q_{out,3}$ is equal to the flow capacity C_3, creating a kinematic wave with speed $-w_3$ and density value ρ_3^c. As a result, the supply function $S_3(t)$ at the entrance of I_3 fluctuates between 0 and C_3, leading the effective supply $\mathcal{E}_1(t)$ to alternate between 0 and $\min\{C_1,\ C_3\}$.

ARTICLE LINK: http://www.sciencedirect.com/science/article/pii/S0968090X15001266
PLEASE CITE THIS ARTICLE AS
Han, K., Sun, Y., Liu, H., Friesz, T.L., Yao, T., 2015. A bi-level model of dynamic traffic signal control with continuum approximation. Transportation Research Part C 55, 409-431.

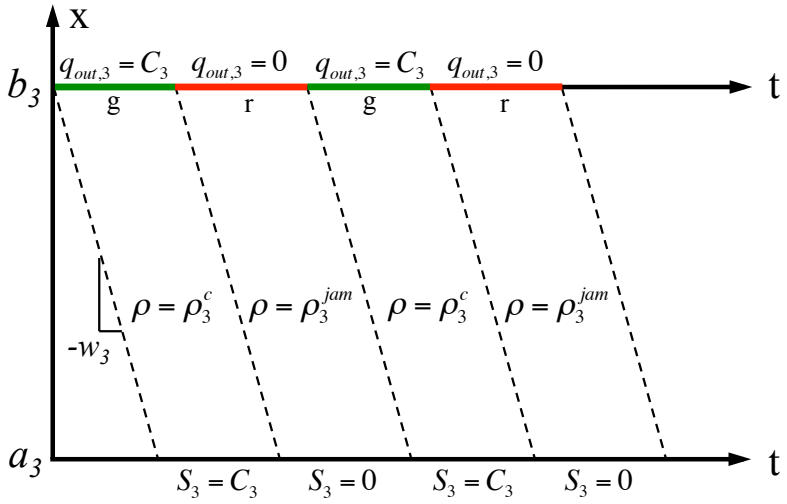

Figure 2: Space-time density diagram for link I_3 when the spillback is sustained at node A, and when a triangular fundamental diagram is employed. The dashed lines represent boundaries between different density values (shocks) traveling backward at speed w_3. C_3 denotes the flow capacity; $q_{out,3}$ denotes the link exit flow; ρ_3^c and ρ_3^{jam} denote respectively the critical density and the jam density; S_3 denotes the supply at the entrance of the link.

The key observation is that the average throughput of I_1 now depends not only on its own green split parameter η_1, but also on the downstream blockage effect characterized by the supply function $S_3(t)$. In other words, it is jointly determined by η_1 and the relative configuration between $u_1(t)$ and $S_3(t)$; thus the continuum signal model as defined by (3.9) alone is no longer sufficient to capture these configurations. To see an example, we stipulate that $u_1(\cdot)$ and $S_3(\cdot)$ are configured in a way such that $S_3(t) = C_3 \cdot u_1(t)$, and perform the following calculation:

$$\int_0^t \mathcal{E}_1(\tau)u_1(\tau)\,d\tau \;=\; \int_0^t \min\{C_1,\, C_3\}\cdot u_1^2(\tau)\,d\tau \;=\; \int_0^t \min\{C_1,\, C_3\}\cdot u_1(\tau)\,d\tau \;=\; \int_0^t \mathcal{E}_1(\tau)\,d\tau$$

which is, by no means, a sound approximation of $\eta_1 \int_0^t \mathcal{E}_1(\tau)\,d\tau$, which is stipulated by the continuum signal model. Moreover, as the cycle length Δ_B for I_3 tends to zero, the supply $S_3(t)$ and the effective supply $\mathcal{E}_1(t)$ do not have bounded variations. As a consequence, the convergence described in Theorem 3.3 no longer holds in this case (see Remark 3.5 below for further discussion). We therefore conclude that in the case of a triangular fundamental diagram, or more generally, FDs with affine congested branch, the proposed continuum junction model does not yield a sound approximation along a corridor that has multiple signal lights interacting with each other in the presence of spillback. However, such a theoretical difficulty may be mitigated by certain choice of fundamental diagrams for I_3, and the key lies in strict concavity.

A strictly concave fundamental diagram $f(\cdot)$ is a piecewise smooth function that satisfies, in addition to **(F)**,

$$f''(\rho) \le -b \qquad \text{for some } \; b \;>\; 0 \tag{3.12}$$

for all $\rho \in [0,\, \rho^{jam}]$ such that $f(\cdot)$ is twice differentiable at ρ. Let us re-visit the scenario where link I_3 is dominated by the congested phase, but assuming a strictly concave fundamental diagram. We begin with the observation that in this case the characteristic field is genuinely nonlinear. As a result, any flux variation generated by signal control at the exit of the link gets instantaneously reduced when the waves propagate backwards, see Bressan (2000) for more mathematical details. Therefore, it is expected that the approximation error becomes significantly smaller than the triangular FD case, and the convergence may still hold even in the presence of sustained spillback, We have the following theorem.

Theorem 3.4. (Han et al., 2014) *In view of Figure 1, and under the same setting and notations of Theorem 3.3, we assume that spillback coming from I_3 is present and sustained at junction A. Then, if the fundamental diagram $f_3(\cdot)$*

of I_3 is triangular or trapezoidal, there holds

$$\left|N_1^{\Delta_A}(t,\,x) - N_1^0(t,\,x)\right| \;\le\; \eta_1(1-\eta_1)\Delta_A \min\{C_1, C_3\} + \min\{C_1,\,C_3\}\,\eta_1 t \tag{3.13}$$

If the fundamental diagram $f_3(\cdot)$ of I_3 is strictly concave, we have

$$\left|N_1^{\Delta_A}(t,\,x) - N_1^0(t,\,x)\right| \;\le\; \eta_1(1-\eta_1)\Delta_A \min\{C_1, C_3\} + \min\left\{C_1,\, f_3\left((f_3')^{-1}\left(\frac{-L_3}{L_3/w_3+\Delta_B}\right)\right)\right\}\eta_1 t \tag{3.14}$$

for all $(t,\,x) \in [0,\,T]\times[a_1,\,b_1]$, where Δ_B denotes the cycle length for link I_3 and L_3 denotes the length of I_3; $f_3(\cdot)$ denotes the strictly concave fundamental diagram of I_3 with $f_3'(\rho_3^{jam}) = -w_3$. In particular, $N_1^{\Delta_A}(t,\,x) \to N_1^0(t,\,x)$ uniformly for all $(t,\,x) \in [0,\,T]\times[a_1,\,b_1]$ as $\Delta_A,\,\Delta_B \to 0$.

Remark 3.5. *In contrast to the triangular case, the convergence result holds for the strictly concave case even in the presence of sustained vehicle spillback. An intuitive explanation, as we mentioned before, is related to the nonlinear effect caused by the strictly concave fundamental diagram. Figure 3 compares the supply profiles observed at the entrance of link I_3 when the whole link is in the congested phase. As $\Delta_B \to 0$, in the triangular case the oscillation in $S_3(t)$ has the biggest amplitude and becomes more and more frequent, causing the total variation to blow up and the convergence to fail. On the other hand, in the strictly concave case the oscillation in $S_3(t)$ is damped as it gets more and more frequent. In fact, one may easily show that the supply $S_3(t)$ has uniformly bounded variation regardless of the cycle length Δ_B (Han et al., 2014). Thus, the convergence continues to hold in this case.*

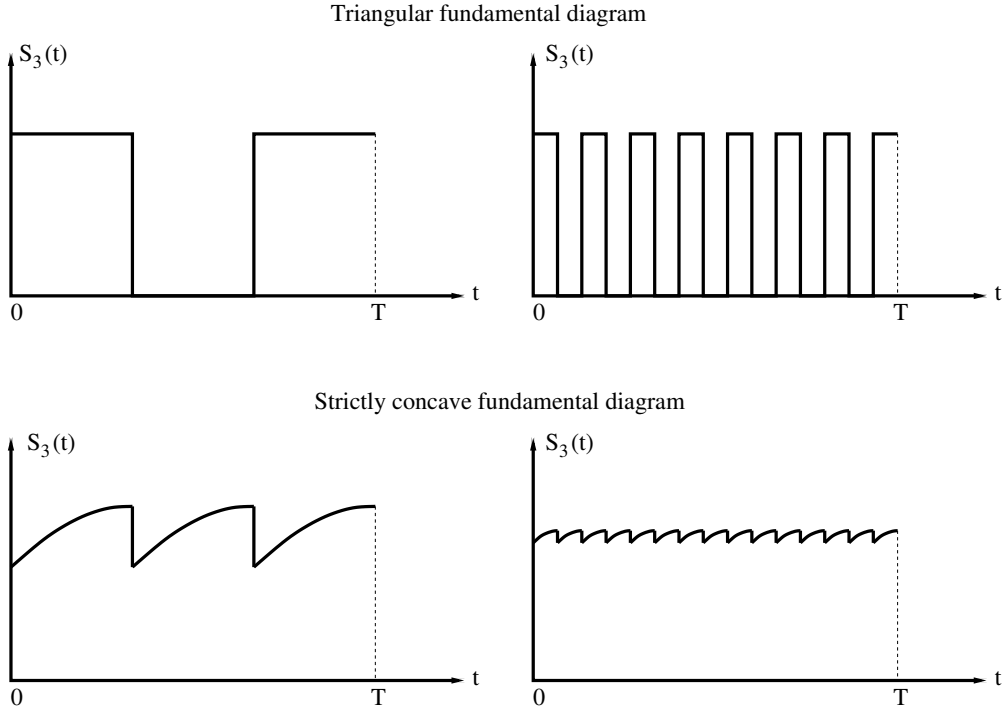

Figure 3: Profiles of the supply observed at the entrance of I_3, when I_3 is dominated by the congested phase and controlled by a signal $u_3(t)$ at the exit. First row: the triangular case; second row: the strictly concave case. First column: larger signal cycle; second column: smaller signal cycle.

Notice that in the presence of sustained spillback, the errors associated with triangular or strictly concave fundamental diagrams both grow with time; see (3.13) and (3.14). However, the error in the strictly concave case is smaller than the triangular case. This is quite clear from Theorem 3.4 and Remark 3.5 and will be numerically verified later in Section 3.4. The main relevant findings made in Han et al. (2014) can be summarized below.

(a) In a signalized network, if no spillback occurs, the difference between the two solutions obtained with the on-and-off model and the continuum model is uniformly bounded and does not grow with time. This is true for any type of fundamental diagram employed.
(b) If sustained spillback occurs, then the above difference may grow with time, regardless of the fundamental diagram. However, when using a strictly concave fundamental diagram, the difference is smaller than when a triangular/trapezoidal fundamental diagram is assumed. In addition, the approximation error is dependent on the length and signal cycle of relevant links.

In this paper, we provide some further insights regarding the approximation error and the choice of the fundamental diagram, based on the previously mentioned findings.

Proposition 3.6. *In view of Figure 1, when sustained spillback occurs at junction A, the approximation error* $|N_1^{\Delta_A}(t,\, x) - N_1^0(t,\, x)|$ *for link* I_1 *decreases with larger* L_3 *and/or smaller signal cycle* Δ_B*, where* L_3 *and* Δ_B *are the length and signal cycle of link* I_3*. Moreover, such an error is determined only by the congested branch of the fundamental diagram of* I_3*.*

Proof. The conclusion follows immediately from the fact that the quantity

$$f_3\left((f_3')^{-1}\left(\frac{-L_3}{\frac{L_3}{w_3}+\Delta_B}\right)\right) \;=\; f_3\left((f_3')^{-1}\left(\frac{-1}{\frac{1}{w_3}+\frac{\Delta_B}{L_3}}\right)\right) \tag{3.15}$$

appearing on the right hand side of (3.14) is a decreasing function of L_3, and an increasing function of Δ_B. Moreover, we observe that (3.15) only relies on knowledge of the congested branch of $f_3(\cdot)$, i.e. where f_3' is negative. □

Proposition 3.6 suggests that the approximation error of the continuum signal model depends, in a quantifiable way, on the length and signal cycle of the link that triggers spillback (e.g., link I_3 in Figure 1). As suggested by these findings, in order to obtain a more accurate approximation of the on-and-off signal model with the continuum signal approximation, one should

1. employ a fundamental diagram with a strictly concave congested branch, where appropriate; and
2. employ the continuum approximation where the link responsible for possible spillback is long, and is controlled by a signal with relatively small cycle length.

Notice that one may choose any functional form for the uncongested branch of the fundamental diagram without affecting the approximation accuracy. For example, it is suitable to choose the piecewise-defined fundamental diagram (3.16) with a linear uncongested branch and a strictly concave congested branch. Such a fundamental diagram is also consistent with some empirical evidence (Papageorgiou et al., 1990).

$$f(\rho) \;=\; \begin{cases} v_0\rho & \rho \in [0,\, \rho^c] \\ g(\rho) & \rho \in (\rho^c,\, \rho^{jam}] \end{cases} \tag{3.16}$$

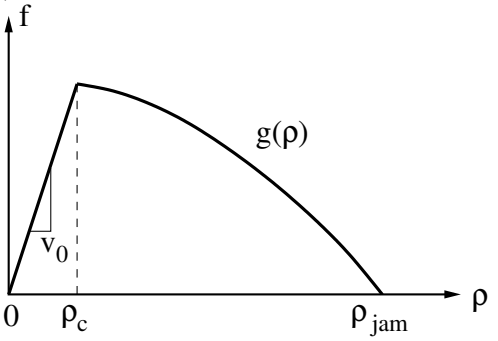

In (3.16), v_0 denotes the free flow speed, ρ^c denotes the critical density, and ρ^{jam} denotes the jam density. The function $g(\cdot)$ satisfies

$$g(\rho^c) \;=\; v_0 \cdot \rho^c\,, \qquad g''(\rho) \;\leq\; -\,c \text{ for some } c \;>\; 0\,, \qquad g(\rho^{jam}) \;=\; 0$$

If the congested branch of the fundamental diagram is piecewise linear instead of strictly concave, then the approximation accuracy can also be improved, especially with more linear pieces in the congested branch. This observation stems from the fact that a strictly concave FD can be approximated by a piecewise linear FD, and the resulting solution can be also approximated via the wave-front tracking method (Dafermos, 1972).

Remark 3.7. *Another type of vehicle spillback, in contrast to the sustained spillback, is transient spillback in which the spillback does not persist at the junction but instead recurs from cycle to cycle. This situation arises when the discharged flows from upstream links are insufficient to keep the entrance of the downstream link congested throughout a cycle. An illustration of the transient spillback is provided in Han et al. (2014). The existence of transient spillback poses additional difficulties to the continuum modeling of signalized junctions regardless of the fundamental diagram employed, although one may argue that modeling these phenomena exactly loses importance in large scale applications. Therefore, this should not completely diminish the value of the continuum signal model in the venue of engineering applications.*

3.4. Implementing the continuum signal model in the DNL procedure: A numerical test

In this section we will conduct a numerical case study to demonstrate the approximation accuracy of the continuum signal model while taking into account a range of contributing factors. These include the fundamental diagram, and the signal cycle and length of the link that triggers spillback, whose effects on the approximation accuracy have been illustrated in Proposition 3.6. The LWR-based DNL model, together with the on-and-off signal model (3.8) or the continuum signal model (3.9), will be employed and compared in this study.

We consider the seven-arc, six-node network shown in Figure 4, with one origin-destination pair (1, 6) and three paths $p_1 = \{I_1, I_2, I_5, I_7\}$, $p_2 = \{I_1, I_2, I_4, I_6, I_7\}$, and $p_3 = \{I_1, I_3, I_6, I_7\}$. The network is controlled by signal lights at the merge nodes 4 and 5. Two types of fundamental diagrams (FDs) are considered for comparison purposes: a triangular FD and a Greenshields (quadratic and thus strictly concave) FD; their parameters are shown in Table 1. Initially, the lengths of all links are set to be 3 (in mile). Later on we will change the length of link I_6 to illustrate its impact on the approximation accuracy of the continuum signal model in the event of spillback.

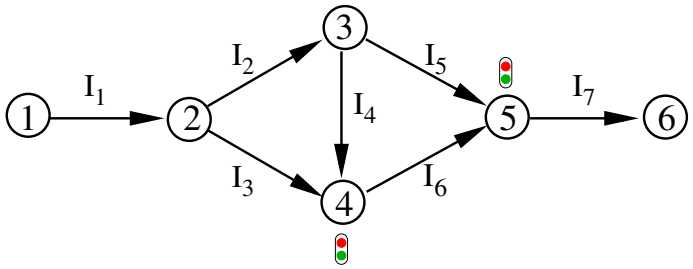

Figure 4: The seven-arc, six-node network

		I_1	I_2	I_3	I_4	I_5	I_6	I_7
Triangular	v_0 (mile/hour)	30	30	30	30	30	30	30
	ρ^{jam} (vehicle/mile)	400	200	400	200	200	200	200
	ρ^c (vehicle/mile)	100	50	100	50	50	50	50
	C (vehicle/hour)	3000	1500	3000	1500	1500	1500	1500
Greenshields	v_0 (mile/hour)	30	30	30	30	30	30	30
	ρ^{jam} (vehicle/mile)	400	200	400	200	200	200	200
	ρ^c (vehicle/mile)	200	100	200	100	100	100	100
	C (vehicle/hour)	3000	1500	3000	1500	1500	1500	1500

Table 1: Link parameters corresponding to the triangular and the Greenshields fundamental diagrams. v_0 denotes the free-flow speed, ρ^{jam} denotes the jam density, ρ^c denotes the critical density, and C denotes the flow capacity.

We fix a time horizon [0, 3] (in hour). Throughout this section, the path departure rates are set to be: $h_1(t) = 400$, $h_2(t) = 1200$, $h_3(t) = 2000$ (in veh/h) for $t \in [0.05, 0.45]$ (in hour); and $h_1(t) = h_2(t) = h_3(t) = 0$ otherwise. We also specify the signal splits at nodes 4 and 5 by setting $\eta_3 = 1/2$, $\eta_5 = 2/3$; by default $\eta_4 = 1 - \eta_3 = 1/2$, $\eta_6 = 1 - \eta_5 = 1/3$.

Given the link parameters in Table 1, one expects node 5 to be a potential bottleneck, causing congestion on link I_6 to accumulate and eventually trigger vehicle spillback at node 4, affecting both I_3 and I_4. In the rest of the section, we will compare the effectiveness of the continuum signal model in approximating the on-and-off model, when the triangular and the Greenshields fundamental diagrams are respectively used. Previously established theoretical results, including Theorem 5.4 of Han et al. (2014), and Proposition 3.6 of this paper, suggest that (1) the Greenshields fundamental diagram will yield a lower approximation error than the triangular FD; (2) for the Greenshields FD, the error grows with larger signal cycle at nodes 5 and/or with shorter length of link I_6. In order to verify these results, we consider three scenarios:

(I) the cycle length at nodes 4 and 5 is equal to 54 s, and the length of I_6 is 3 miles;

(II) the cycle length at nodes 4 and 5 is equal to 54 s, and the length of I_6 is 1.5 miles;

(III) the cycle length at nodes 4 and 5 is equal to 108 s, and the length of I_6 is 1.5 miles.

Figures 5-7 show, for Scenarios I, II, and III respectively, the cumulative exit vehicle counts of I_3 and I_4, which are affected by the possible spillback at node 4 triggered by link I_6. From these figures, we see that the continuum model with the triangular FD misinterprets the dynamics predicted by the exact on-and-off model. In particular, for all three scenarios there exists a period in the [triangular + on-and-off] case where the throughput of I_3 is zero, as can be seen from the flat part in the cumulative exit vehicle counts. The reason for the zero throughputs is that, when a sustained spillback occurs at node 4, the signal control $u_3(t)$ for I_3 and the supply $S_6(t)$ of I_6 are configured in a way such that $u_3(t) = 0$ whenever $S_6(t) = C_6$ (see the discussion at the beginning of Section 3.3.2). Thus the discharged flow from I_3 is effectively zero in the duration of the spillback. The [triangular + continuum] case, on the other hand, predicts a positive discharge flow from I_3 during the spillback, and thus does not capture well the throughput of I_3. As a result, use of the triangular FD yields significant discrepancies in the vehicle counts, with the biggest being 200+ (vehicles). In contrast, the Greenshields case yields a much smaller error during spillback in all three scenarios, due to the strict concavity in the FD as we illustrated in Theorem 3.4 and Remark 3.5. In addition, within the Greenshields case we see a worsening of the approximation quality from Scenario I $\rightarrow$ II $\rightarrow$ III, which is consistent with the findings made in Proposition 3.6 and the discussions presented thereafter.

Figures 8-10 show, for Scenarios I, II, and III respectively, the path travel times, which are the main outputs of the DNL procedure. One may similarly conclude that using the strictly concave (Greenshields) FD yields improved continuum approximation than the triangular FD, when spillback is present.

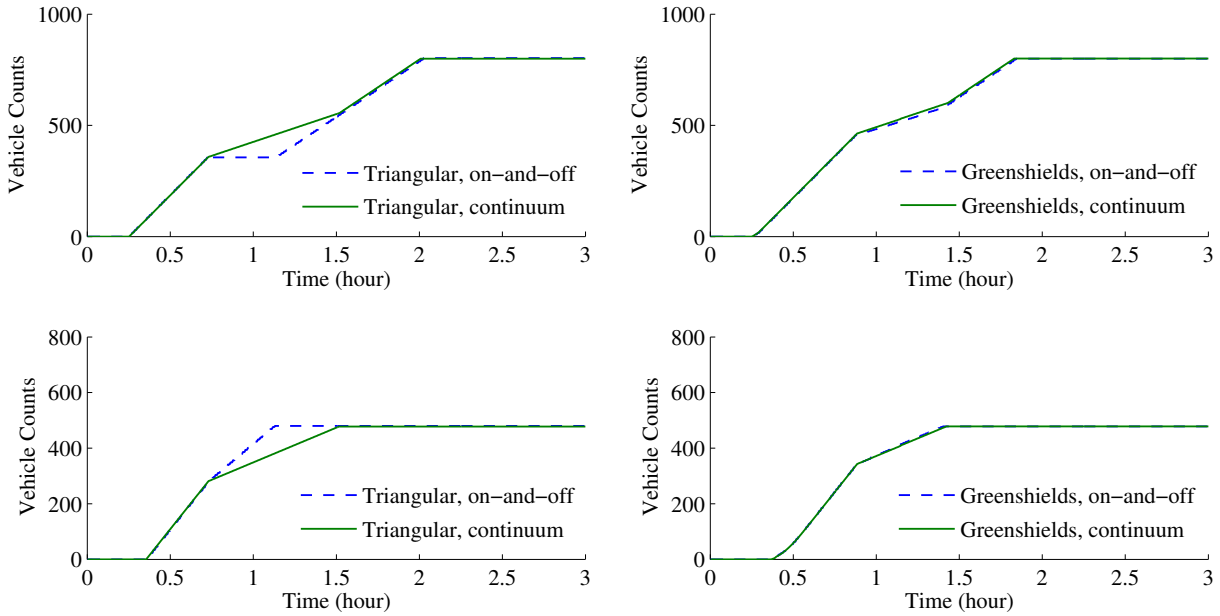

Figure 5: Exiting vehicle counts of links I_3 and I_4 in Scenario I. First row: link I_3; second row: link I_4. Left column: triangular case; right column: Greenshields case.

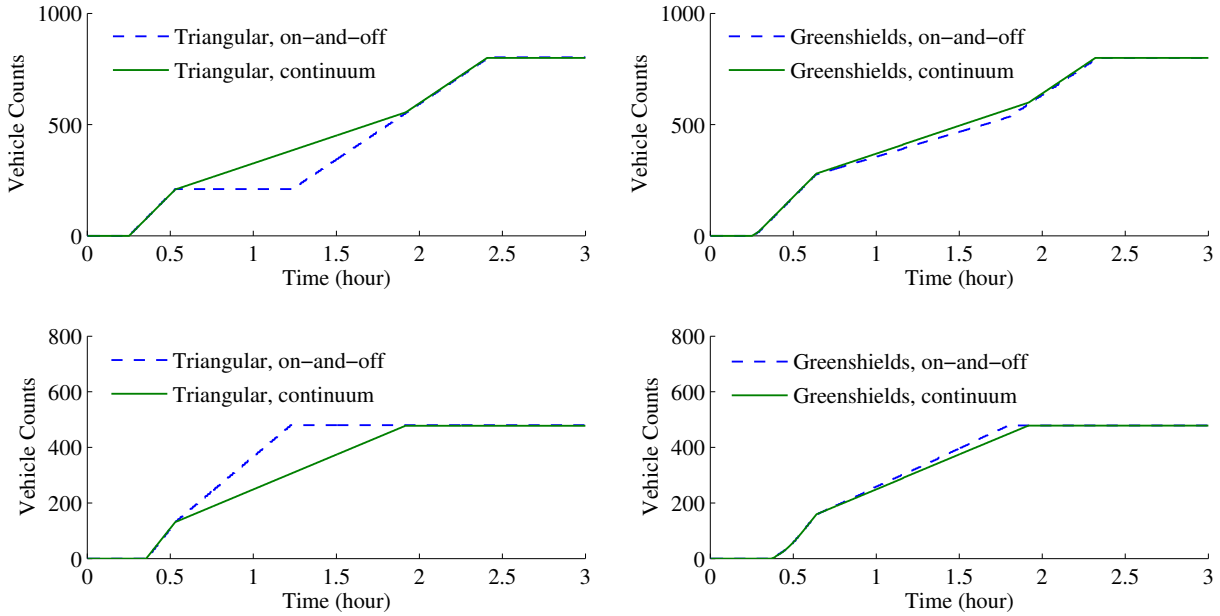

Figure 6: Exiting vehicle counts of links I_3 and I_4 in Scenario II. First row: link I_3; second row: link I_4. Left column: triangular case; right column: Greenshields case.

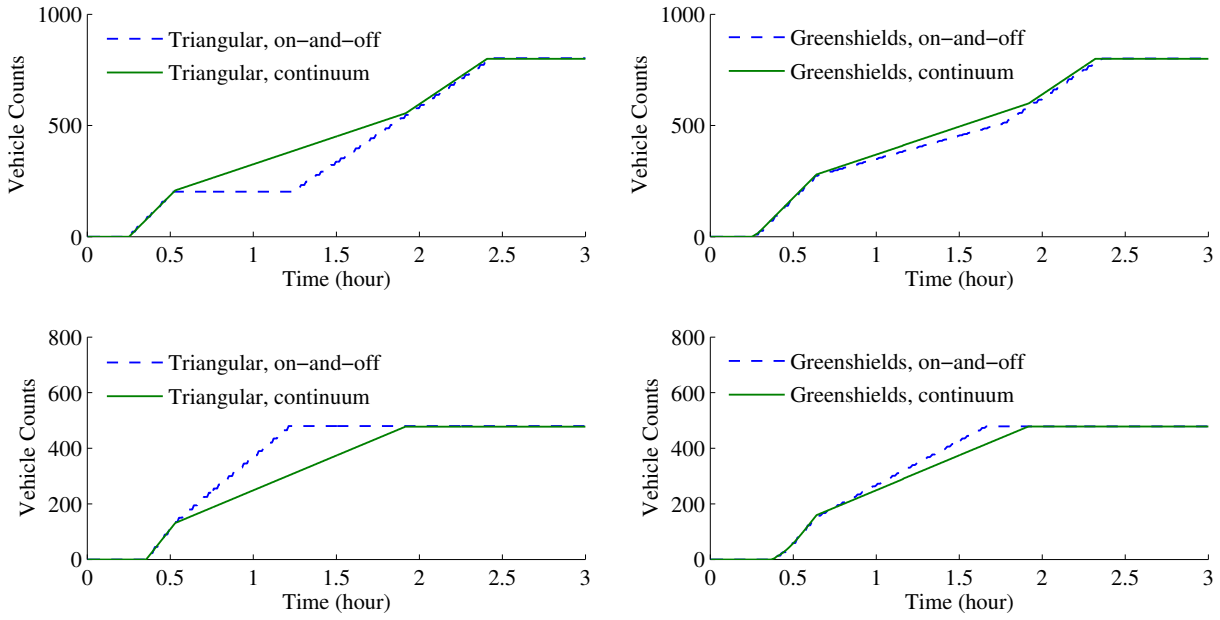

Figure 7: Exiting vehicle counts of links I_3 and I_4 in Scenario III. First row: link I_3; second row: link I_4. Left column: triangular case; right column: Greenshields case.

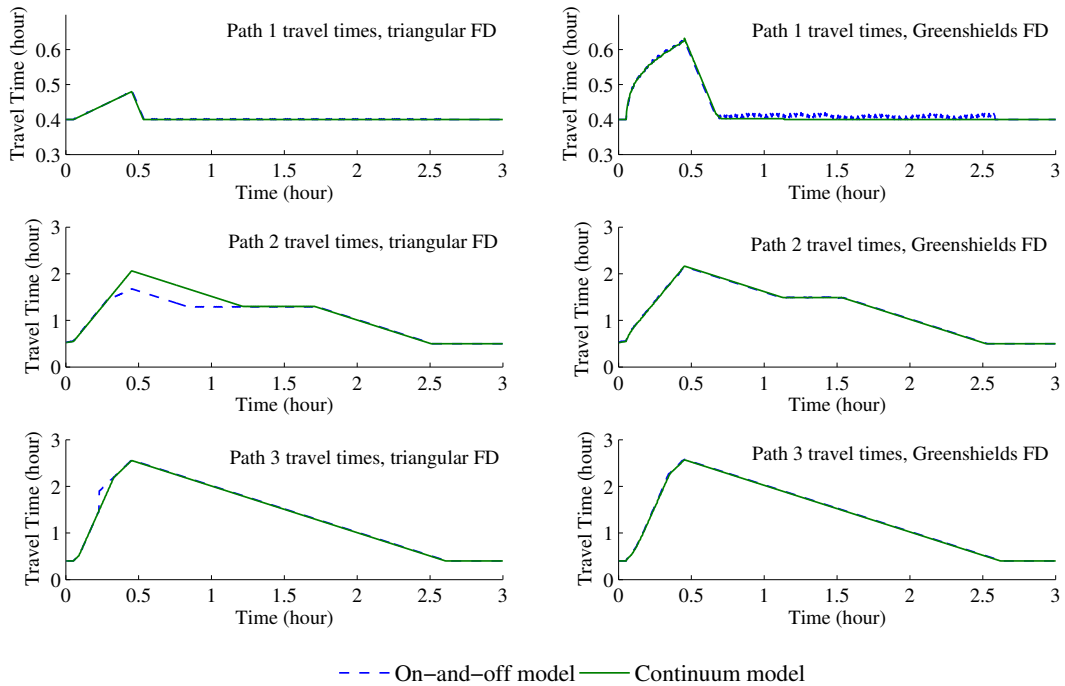

Figure 8: Comparison of path travel times in Scenario I. Top row: path 1; middle row: path 2; bottom row: path 3. Left column: triangular case; right column: Greenshields case.

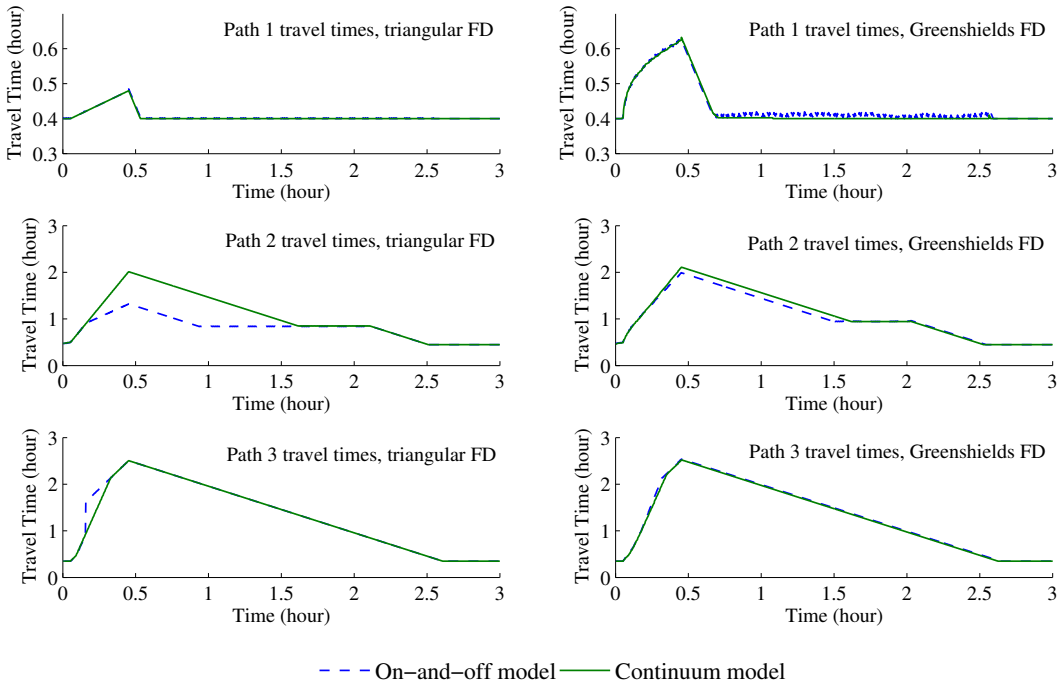

Figure 9: Comparison of path travel times in Scenario II. Top row: path 1; middle row: path 2; bottom row: path 3. Left column: triangular case; right column: Greenshields case.

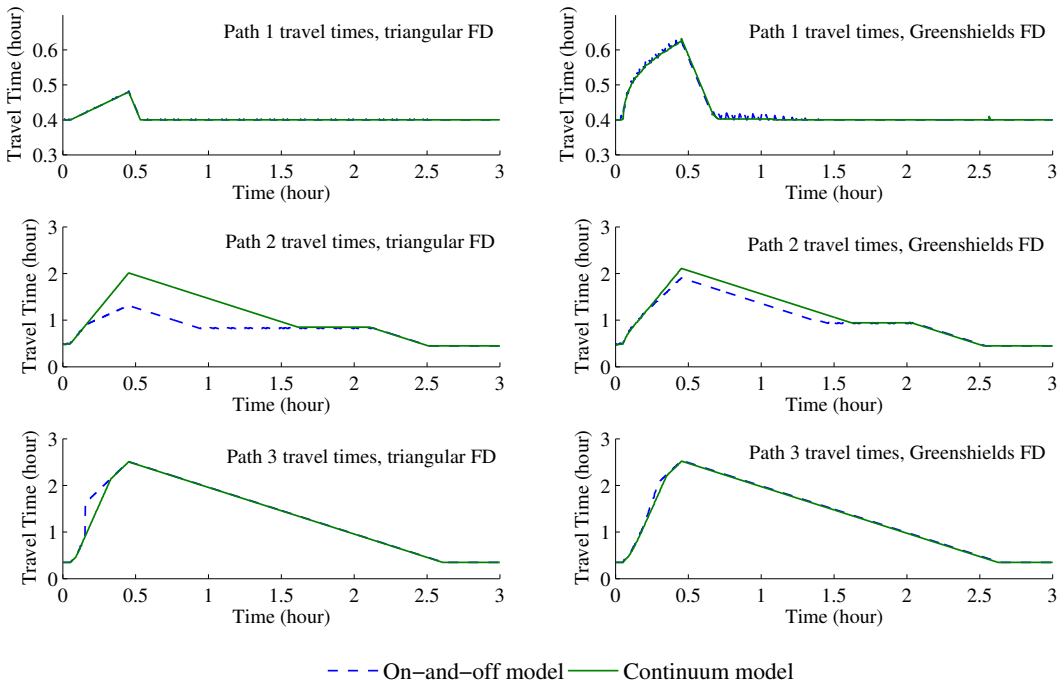

Figure 10: Comparison of path travel times in Scenario III. Top row: path 1; middle row: path 2; bottom row: path 3. Left column: triangular case; right column: Greenshields case.

4. Signal control problem formulated as a mathematical program with equilibrium constraints

The proposed bi-level signal control problem is expressed as an optimization problem with an objective typically involving the minimization of network-wide travel costs, and with the lower-level dynamic user equilibrium (DUE) problem expressed as constraints. In our upper-level problem, the decision variables are the signal green splits that are embedded within the continuum signal model in the dynamic network loading (DNL) sub-problem of DUE. We denote by the vector $\eta(t)$ the possibly time-varying signal green splits associated with the entire network. The obvious dependence of the DNL procedure on these signal splits is indicated in the following notation:

$$\Psi(t,\, h;\, \eta) \;=\; \Big(\Psi_p(t,\, h;\, \eta),\quad p \in \mathcal{P}\Big) \qquad \eta(t) \in Y$$

where Y denotes the set of feasible signal splits. In this paper we stipulate that the sum of the green splits associated with all incoming approaches of the same junction is equal to one at any time. However, in some cases the sum can be less or greater than one, depending on the detailed signal phasing plans. For example, if there is a pedestrian phase or all-red phase, then the sum is less than one. If there exists a signal stage with two or more non-conflicting streams from different approaches, then the sum of green splits may be larger than one. These complications will not be elaborated in this paper. Notice that the feasible set Y may be further shaped by minimal green/red times, pedestrian phase, traffic safety and equity, etc.

The lower-level dynamic user equilibrium problem with a given signal timing $\eta(t)$ is formulated as the following variational inequality.

$$\left.\begin{array}{c} \text{find } h^* \in \Lambda \text{ such that} \\ \displaystyle\sum_{p\in\mathcal{P}} \int_{t_0}^{t_f} \Psi_p(t,\, h^*;\, \eta)(h_p(t) - h_p^*(t))dt \;\geq\; 0 \\ \forall h \in \Lambda \end{array}\right\} VI(\Psi,\, \Lambda,\, \eta,\, [t_0,\, t_f]) \tag{4.17}$$

where Λ is defined in (2.3). The objective of the upper-level problem is to minimize the total travel costs on the entire network, through the controls $\eta(t)$. This is formulated as

$$\min_{\eta(t)\in Y} \sum_{p\in\mathcal{P}} \int_{t_0}^{t_f} \Psi_p(t,\, h^*;\, \eta) h_p^*(t) dt$$

where h^* is determined by the VI problem (4.17). To sum up, the mathematical program with equilibrium constraints (MPEC) formulation of the proposed bi-level dynamic signal control problem is given as follows.

$$\min_{\eta(t)} \sum_{p\in\mathcal{P}} \int_{t_0}^{t_f} \Psi_p(t,\, h^*;\, \eta) h_p^*(t)\, dt \tag{4.18}$$

$$\text{subject to} \quad \left\{\begin{array}{ll} \displaystyle\sum_{p\in\mathcal{P}} \int_{t_0}^{t_f} \Psi_p(t,\, h^*;\, \eta)(h_p(t) - h_p^*(t))dt \;\geq\; 0 & \forall h \in \Lambda \\ h^* \in \Lambda, \quad \eta(t) \in Y & \end{array}\right. \tag{4.19}$$

We make three observations regarding this MPEC. (1) The variational inequality poses a semi-infinite constraint to the optimization problem because the inequality has to be satisfied for infinitely many departure flow vectors $h \in \Lambda$. In other words, this inequality constraint has an infinite index set. (2) The delay operator $\Psi(t,\, h;\, \eta)$ enjoys very little regularity with respect to any of its arguments or parameters. This is caused by the presence of shock waves (discontinuities in vehicle density and flow) inherent in the LWR model, as well as the non-differentiable algebraic equations expressing the continuum signal junction model (3.9). (3) The equilibrium constraints expressed by the VI is nonconvex. To illustrate (2) and (3) with visualization, we consider again the seven-arc, six-node network depicted in Figure 4 where the continuum signal control variables are $\eta_3(t)$ and $\eta_5(t)$. We set both $\eta_3(t)$ and $\eta_5(t)$ to be time-independent and reduce the control space to a subset of the two-dimensional plane. We then calculate the objective values (4.18) for a range of control values η_3 and η_5, by solving DUE problems with the following network configuration:

1. Only node 4 and 5 are signalized intersections.
2. The O-D demand is 1000 (vehicles).
3. The signal splits at nodes 4 and 5 for each incoming link are time-independent, chosen within the interval [0.2, 0.8].
4. The Greenshields fundamental diagram is used for all links, with parameters given in Table 1.

From these calculations a two-dimensional surface representing the objective function is constructed as shown in Figure 11. We observe that the objective function is indeed nonconvex in its two decision variables, and that the regularity of the objective function is poor. If η_3 and η_5 are time-varying, the problem becomes even more complex and difficult to visualize, but observations (2) and (3) will remain valid.

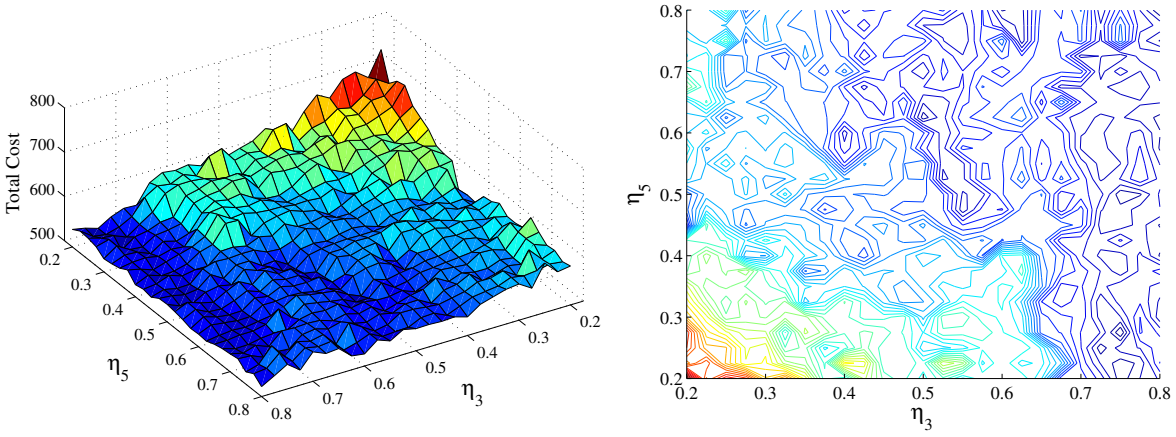

Figure 11: Visualization of the simplified MPEC problem. Left: the surface representing the objective function; right: the contour plot of the surface on the left.

In view of the observations made above, we will employ metaheuristic solution methods for the MPEC. A metaheuristic method, although enjoying less rigorous results regarding convergence, solution quality and overall performance, has a few distinctive advantages over exact methods. Firstly, it usually does not assume knowledge beyond the zeroth-order information of the objective function and constraints. As a result, it usually entails a considerably reduced per-iteration complexity in comparison with methods that utilize the first-order (gradient) and second-order (Hessian) information (for example, the gradient descent algorithm and the interior point algorithm). This allows metaheuristic algorithms to be naturally applied to complex optimization problems whose first- and second-order information is hardly available. Secondly, in large-scale engineering applications, the exact global optimal solution is often of secondary importance compared to a "coarsely optimized" solution obtained yet in a timely fashion. Metaheuristic algorithms can often be terminated at any time to satisfy user-defined time constraint, and provide some useful improvements to the system of interest.

In this paper, we consider three metaheuristic algorithms: *particle swarm optimization* (PSO), *simulated annealing* (SA), and *nested partition* (NP). A short introduction to these metaheuristics is provided below.

4.1. Simulated annealing

Simulated annealing (SA) is a probabilistic search method proposed by Kirkpatrick et al. (1983) and Černý (1985) for nonconvex optimization. This method imitates the physical process of natural annealing, i.e. a material cools down from a high temperature to a relatively low temperature, reaching a minimal energy crystalline structure. Within such imitation, the SA algorithm randomly generates and randomly accepts new solutions. More specifically, at each iteration, a random perturbation to the current solution is made to generate a new solution. If the new solution improves the current solution, this new solution is accepted and replaces the current solution; otherwise, the new solution is accepted according to a certain probability. This probability is determined by the current temperature T_{SA}, and decreases as T_{SA} gets lower. During early iterations when T_{SA} is relatively high, acceptance of non-improving solutions

is more likely to happen; as T_{SA} decreases after several iterations, acceptance of a new solution becomes more difficult. The algorithm terminates when the temperature drops below a prescribed level. The following pseudocode for SA is presented, where we use $\mathcal{U}(\cdot)$ to denote the objective function.

Pseudocode for simulated annealing

Input Fix $\alpha \in (0, 1)$, and the terminal temperature $T_{terminal} > 0$. Fix a positive integer $\mathcal{L}$.

Step 0. Start with a feasible solution $x^{current}$. Initialize the temperature $T_{SA} > T_{terminal}$. Denote by x^{best} the best solution so far and let $x^{best} = x^{current}$. Set $k = 0$.

Step 1. Perturb from the current solution $x^{current}$ to find a different feasible solution x^{trial}.

Step 2. If $\mathcal{U}(x^{trial}) < \mathcal{U}(x^{current})$, accept state x^{trial} and let $x^{current} = x^{trial}$. Otherwise, compute the transition probability

$$Prob = \exp\left(\frac{\mathcal{U}(x^{current}) - \mathcal{U}(x^{trial})}{T_{SA}}\right) \tag{4.20}$$

Randomly generate r uniformly within [0, 1]. If $r < Prob$, accept state x^{trial} and let $x^{current} = x^{trial}$.

Step 3. Update the best solution so far, i.e., if $\mathcal{U}(x^{trial}) < \mathcal{U}(x^{best})$, let $x^{best} = x^{trial}$.

Step 4. If $k < \mathcal{L}$, let $k = k + 1$ and go to Step 1. Otherwise go to Step 5.

Step 5. If $T_{SA} \leq T_{terminal}$, the algorithm terminates with output x^{best}. Otherwise, set $k = 0$ and $T_{SA} = \alpha T_{SA}$; go to Step 1.

4.2. Particle swarm optimization

Particle swarm optimization (PSO) is a metaheuristic optimization algorithm first introduced by Kennedy and Eberhart (1995), based on the social behavior of a group of animals such as a flock of birds or a school of fish, both called a *swarm*. In a swarm, the animals are represented as particles, and can collaborate and share information to adjust their positions in the search for a certain location. The adjustment of their positions is based on the swarm's collective memory on the best location attained so far (subsequently referred to as "gbest"), and the individual memory of the best location that the individual particle has attained so far (referred to as "pbest"). As a result of the position adjustment, the particles tend to converge to either "gbest" or "pbest". Compared with other algorithms or approaches based on natural paradigms, such as simulated annealing, genetic algorithms and artificial neural networks, PSO is relatively new and still emerging. However, it has gained much popularity among researchers and has been applied to many domains of application with great success (Banks et al., 2007). Although the performance of PSO varies depending on the application or parameters chosen, research shows evidences of PSO or its variations outperforming well-established metaheuristics such as genetic algorithm, ant colony optimization, simulated annealing, and tabu search (Yin, 2006; Savsani et al., 2010; Sha and Hsu, 2007).

The canonical PSO process for minimizing an objective function $\mathcal{U}(\cdot)$ within a feasible region $S \subset \mathbb{R}^n$ can be represented as the following discrete dynamics:

$$V_i^{k+1} = \omega_k V_i^k + c_1 r_1 (P_i^k - X_i^k) + c_2 r_2 (G^k - X_i^k), \quad \forall i, k \tag{4.21}$$

$$X_i^{k+1} = P_S[X_i^k + V_i^{k+1}], \quad \forall i, k \tag{4.22}$$

where X_i^k, $V_i^k \in \mathbb{R}^n$ denote the position and velocity of the i-th particle at the k-th iteration, respectively; $P_i^k \in \mathbb{R}^n$ is the "pbest" of the i-th particle so far until the k-th iteration; and $G^k \in \mathbb{R}^n$ is the "gbest" of the entire swarm so far until the k-th iteration. $\omega_k \in (0, 1)$ is the *weight of inertia*, which maintains certain level of consistency between the velocities in two consecutive iterations. Constants c_1 and c_2 are the *acceleration rates*, which determine the impacts of the individual memory "pbest" and the swarm's collective memory "gbest" on the decision at the current iteration.

The larger the c_1 and c_2, the faster the particles move towards the memorized best locations. r_1 and r_2 are random numbers with a uniform distribution in [0, 1] generated at each iteration. $P_S : \mathbb{R}^n \to S$ is the Euclidean projection, defined as $P_S[x] \doteq \text{argmin}_{y\in S}\|x - y\|$. Eqns (4.21)-(4.22) are iterated, while "pbest" and "gbest" are updated at each iteration. Such a procedure can be interpreted as a multi-start, zeroth-order (derivative-free) optimization heuristic. The velocities $\{V_i^k\}$ can be regarded as potential descent directions determined by sampling feasible candidate solutions. Intuitively, solutions in the neighborhood of "pbest" and "gbest" hold promise in achieving better objective values, thus the potential descent direction determined by the PSO is a combination of the directions from the current particle location to "pbest" $(P_i^k - X_i^k)$, and to "gbest" $(G^k - X_i^k)$, plus an additional deviation term $\omega_k V_i^k$. During early iterations, the PSO tends to sample uniformly the entire feasible region. As the swarm gradually "migrates" along the potential descent directions, the particles tend to gather around either the "pbest" or the "gbest", so that the neighborhoods of the "pbest" and the "gbest" are sampled more intensively. The algorithm usually terminates when no more improvement of the objective is attained for a given number of iterations. A pseudocode of the PSO is given below, where $\mathcal{U}(\cdot)$ denotes the objective function.

Pseudocode for particle swarm optimization

Input. Choose a population size $Pop > 0$. Fix $\{\omega_k : k \geq 0\} \subset (0, 1)$, $c_1, c_2 > 0$.

Step 0. Let $k = 0$. Initialize randomly the particle locations X_i^0 and velocities V_i^0, $1 \leq i \leq Pop$. Initialize "pbest" P_i^0 and "gbest" G^0 as follows:

$$P_i^0 = X_i^0 \quad 1 \leq i \leq Pop, \qquad\qquad G^0 = P_{i^*}^0$$

where $i^* = \underset{1\leq i\leq Pop}{\text{argmin}}\, \mathcal{U}(P_i^0)$.

Step 1. Update the velocities and positions of the particles. That is, for all $1 \leq i \leq Pop$,

$$V_i^{k+1} = \omega_k V_i^k + c_1 r_1 (P_i^k - X_i^k) + c_2 r_2 (G^k - X_i^k), \qquad X_i^{k+1} = P_S[X_i^k + V_i^{k+1}]$$

where r_1 and r_2 are random numbers uniformly generated within [0, 1].

Step 2. Find the objective values $\mathcal{U}(X_i^{k+1})$ for all $1 \leq i \leq Pop$.

Step 3. Update "pbest" and "gbest":

$$P_i^{k+1} = \begin{cases} X_i^{k+1} & \text{If } \mathcal{U}(X_i^{k+1}) < \mathcal{U}(P_i^k) \\ P_i^k & \text{Otherwise} \end{cases} \qquad \forall 1 \leq i \leq Pop$$

$$G^{k+1} = \begin{cases} P_{i^*}^{k+1} & \text{If } \min\limits_{1\leq i\leq Pop} \mathcal{U}(P_i^{k+1}) < \mathcal{U}(G^k) \\ G^k & \text{Otherwise} \end{cases}$$

where $i^* = \underset{1\leq i\leq Pop}{\text{argmin}} \mathcal{U}(P_i^{k+1})$

Step 4. If the stopping criterion is met (e.g. no improvement in the objective within a given number of consecutive iterations), terminate the algorithm with output G^{k+1}. Otherwise, let $k = k + 1$, and go to Step 1.

4.3. Nested partition

The nested partition (NP) method systematically partitions a feasible region and selects promising subregions through random sampling and local search until a singleton is reached. It has been found to be effective in solving large-scale problems in many applications (Al-Shihabi et al., 2008; Shi and Ólafsson, 2000a,b; Shi et al., 2011).

At each iteration of the NP algorithm, the feasible region is divided into two subsets heuristically; one called "*most promising*" and the other called "*complimentary*". The algorithm then further partitions the "most promising" subset into M smaller subregions. Together with the "complimentary" region, the algorithm now divides the feasible domain into $M + 1$ subsets. From each subset a fixed number of points are randomly sampled, and their objective values are used to determine a *promising index* for this subset. The subset with the highest promising index is then selected as the "most promising" set, and is subject to further partitions following the same procedure described above. A backtracking mechanism is incorporated to explore the "less promising" regions. The pseudocode for NP is summarized as follows.

Pseudocode for nested partition

Input. Fix a positive integer M. Denote by $S \subset \mathbb{R}^n$ the feasible domain.

Step 0. Let $k = 0$ and randomly select a non-empty subset R^k of S. Let $P = R^k$ ("most promising" set) and $C = S \setminus P$ ("complementary" set).

Step 1. Randomly partition P into M non-empty subsets $\{P_i\}_{1\le i\le M}$. Randomly sample a fixed number of points from each of the $M + 1$ subsets of S (M subsets of P, plus C) and calculate their objective values. For each subset P_i, define its "promising" index as the best (lowest) objective value, denoted $\mathcal{U}_i^*$, $1 \le i \le M$. For C, define its "promising" index as the best (lowest) objective value, denoted $\mathcal{U}_c$.

Step 2. If $\min_{1\le i\le M} \mathcal{U}_i^* < \mathcal{U}_c$, let $R^{k+1} = P_{i^*}$ where $i^* = \text{argmin}_{1\le i\le M}\mathcal{U}_i^*$; define $P = R^{k+1}$ and $C = S \setminus P$; and continue to Step 3. Otherwise, set $P = R^{\max\{0,k-1\}}$ and $C = S \setminus P$ and go to Step 1.

Step 3. The algorithm terminates if no improvement in the objective value is made within a given number of iterations (indicated by k); otherwise, let $k = k + 1$ and go to Step 1.

5. Numerical examples

5.1. Seven-arc network with constant signal splits

We first test the proposed bi-level model and solution algorithms on the seven-arc network shown in Figure 4. For this study we stipulate that the signal splits η_3 and η_5 are constant throughout the time horizon, and all the network configurations are identical to those employed earlier in the construction of Figure 11. By doing so we have made available a priori knowledge about the global optimum, thus it is possible to evaluate the performance of the three metaheuristics in terms of their solution quality and optimality.

Before we present the computational results obtained from the three metaheuristics, we first provide an informal illustration of the bi-level problem at hand. As shown in Figure 11, the network is at its worst performance when both η_3 and η_5 are small and close to their lower bounds (0.2). This makes sense as in this case most of the road capacity was allocated to links I_4 and I_6, in other words, to path p_2, which has the longest free-flow time and is the least efficient route in the network. Therefore, such a signal timing plan makes the network more restricted and less efficient. Next, we notice that the total network cost is uniformly low when $\eta_3 \in [0.7, 0.8]$, regardless of the value for η_5. This suggests that allocating more green time to the major approach I_3 (link I_3 has a flow capacity of 3000 veh/h while others have only 1500 veh/h) improves the performance of the traffic system, at least locally. This straightforward observation is somehow complicated by the fact that there exist a number of local minima, shown as canyons or basins in the 3-D graph, which yield nearly the same objective value for smaller η_3. This suggests the existence of a Braess-type paradox in which restraining links with the highest capacity (I_3) does not necessarily worsen the overall network performance. This example, despite its simple and low-dimensional nature, reveals the complexity of the MPEC problem and the non-trivial decisions to be made on relevant signal timings. Moreover, such complexity is expected to grow when the dimension of the decision space increases, i.e., when the signal splits become time-varying and/or the underlying network becomes larger.

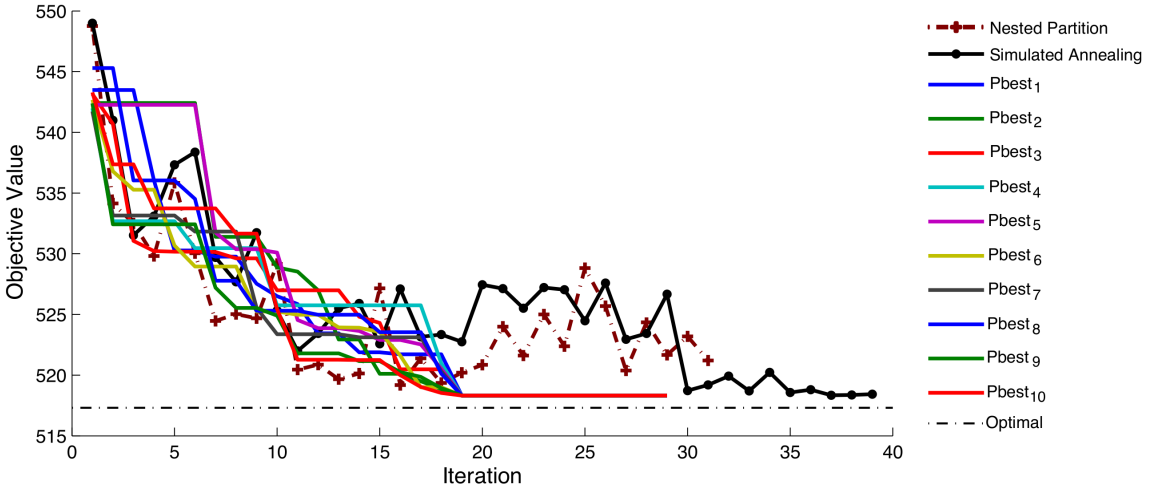

Figure 12: Objective values generated at each intermediate iteration of the three algorithms. 'NP' and 'SA' stand for nested partition and simulated annealing, respectively. Pbest_i, where $1 \le i \le 10$, is the best objective value obtained at the current iteration by the i-th agent employed by PSO. 'Optimal' is the known global optimal value.

We employ the three heuristic algorithms to seek solutions of the nonconvex MPEC with good quality. In Figure 12 we show and compare intermediate objective values generated by the algorithms at each iteration. From this figure, we can observe the search patterns of these three algorithms. In particular, 'Pbest_1-Pbest_{10}' are concerned with the particle swarm optimization, which employs 10 search agents. Each 'Pbest_i' represents the search history of a single agent i ($1 \le i \le 10$). At the beginning, these 10 agents had varied objective values, but they quickly converged to the same objective value within 20 iterations. For the nested partition (NP) and simulated annealing (SA), their objective values show an descending trend overall but with local fluctuations.

All three algorithms achieve close-to-optimal objective values upon termination, where the theoretical optimal objective is calculated a priori through the construction of the objective surface as shown in Figure 11. More accurately, the global minimum is 517.3, and both PSO and SA attain an objective value of 518.3, which has a relative global optimality gap of 0.19%[2]. They are followed by NP, which produces an objective value of 519.1 and a relative global optimality gap of 0.35%. It can be seen that all three methods reach satisfactory solution optimality.

5.2. *Seven-arc network with time-varying splits*

In this numerical example, we set the time horizon to be 5 h and each signal split to be time-varying and change its value every 30 min. One of the goals of this numerical study is to perform a sensitivity analysis for SA and PSO with respect to their parameters. More specifically, the following parameters are considered.

1. We test SA with different combinations of $T_{terminal}$ and $\mathcal{L}$, where $T_{terminal} \in \{10,\ 20,\ 40,\ 80\}$ denotes the terminal temperature, and $\mathcal{L} \in \{5,\ 10,\ 15\}$ is the number of replications performed at each level of temperature. The initial temperature $T_{initial} = T_{terminal} + 80$ and $\alpha = (T_{terminal}/T_{initial})^{0.01}$; see the SA pseudocode for the definition of these parameters.
2. We test PSO with different choices of the acceleration rates $c_1 = c_2 \in \{0.2, 0.6, 1.0, 1.4\}$ and the weight of inertia $\omega_k \in \{0.2, 0.5, 0.8\}$, while fixing the population size to be $Pop = 20$.

The test results are presented in Figures 13 and 14. From Figure 13 regarding SA, we notice three choices of the parameters that yield relatively good performance, namely $(T_{terminal}, \mathcal{L}) \in \{(10, 5), (40, 10), (40, 15)\}$. The first one is more preferred among these three as it yields the minimal average cost, and its upper bound is among the smallest.

[2]Calculated by $\frac{\text{Computed Objective Value}-\text{Global Minimum}}{\text{Global Minimum}} \times 100\%$

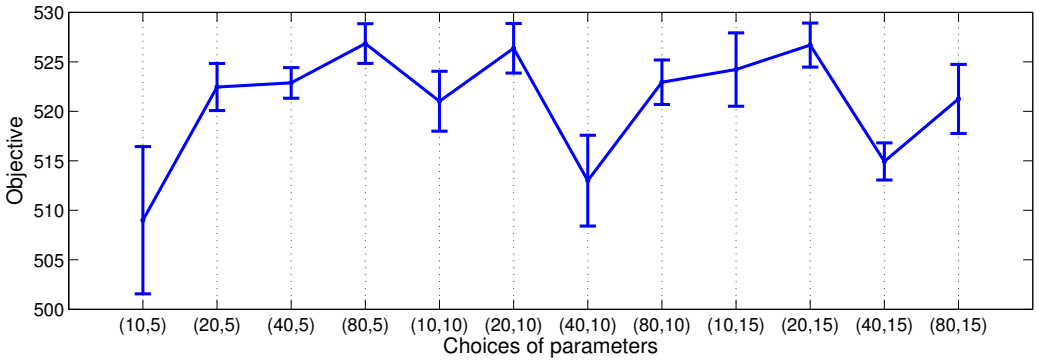

Figure 13: Tuning the parameters in SA. The horizontal axis presents 12 choices of the algorithm parameters ($T_{terminal}$, $\mathcal{L}$). The vertical axis shows the objective values attained. For each choice of the parameters, the vertical bar represents the confidence interval for the average objective value with 90% confidence level.

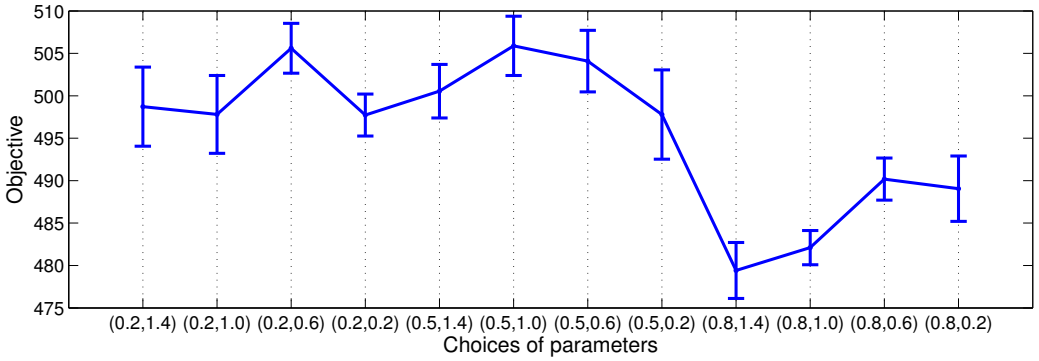

Figure 14: Tuning the parameters in PSO. The horizontal axis presents 12 choices of the algorithm parameters (ω_k, c_1) (recall that $c_1 = c_2$). The vertical axis shows the objective values attained. For each choice of the parameters, the vertical bar represents the confidence interval for the average objective value with 90% confidence level.

Moreover, since it requires the least number of replications $\mathcal{L} = 5$ at each temperature level, this choice results in less computational cost than the other two. From Figure 14 regarding PSO, we notice two good choices of parameters $(\omega_k, c_1) \in \{(0.8, 1.4), (0.8, 1.0)\}$, among which we prefer (0.8, 1.4) as it generates both a lower average cost and a lower upper bound than the other one.

We now compare the tuned SA and PSO with NP. Each algorithm has been repeated 30 times to gain some statistical significance as each algorithm involves stochasticity to some extent. For the PSO and NP, the optimization procedure is terminated once there is no improvement in the objective value in 10 consecutive iterations. The results are presented in Table 2. We observe from this table that PSO substantially outperforms both SA and NP in terms of solution optimality, and the SA uses the least amount of time to reach convergence. In addition, we can clearly see that by allowing the signal timings to be time-varying (that is, to be adaptive to the dynamic traffic flows in the network), the total network travel cost under equilibrium can be reduced from 517.3 (see Figure 12) to 479.4 (PSO), with a 7.3% reduction.

We also compare the acquired solutions with two simple and intuitive signal timing plans in order to highlight the significance of the proposed bi-level approach and the complexity of the decision-making environment. The first alternative signal timing allocates green times equally to all the incoming approaches (indicated as 'Equal' in Table 2 and Table 3); the second timing plan allocates green times that are proportional to the saturation flow (flow capacity) of each incoming approach (indicated as 'Capacity' in Table 2 and Table 3). Table 2 shows that the best heuristic solution, given by PSO, yields on average 14.6% improvement over 'Equal' and 11.7% improvement over 'Capacity'. Finally, Figure 15 shows the time-varying green splits for I_3 and I_5, which are the best solutions obtained from PSO.

Algorithm	Best obj.	Worst obj.	Aver. obj.	CPU time (s)
SA	488.9	532.9	509.0	991
NP	497.8	550.4	527.1	3384
PSO	472.7	497.7	479.4	2529
Equal	561.4	561.4	561.4	—
Capacity	542.8	542.8	542.8	—

Table 2: Optimization results for the 7-arc network.

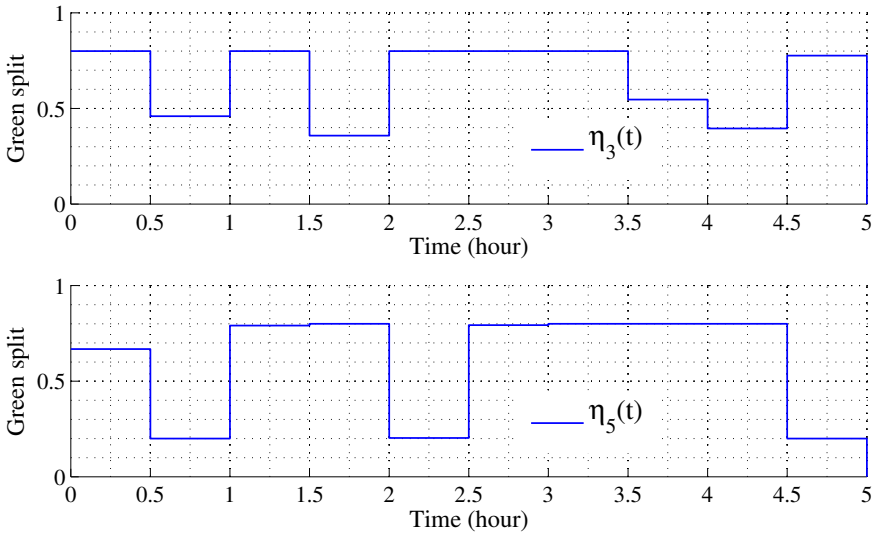

Figure 15: Seven-arc network: The best time-varying solutions for $\eta_3(t)$ and $\eta_5(t)$ obtained from PSO.

5.3. The Sioux Falls network

The bi-level problem is tested on a larger network; namely the Sioux Falls network (see Figure 16). We select 6 origin-destination pairs and 119 paths for the lower-level DUE problem. All intersections in this network are assumed to be signalized, and the signal splits are assumed to change every 15 min. The optimization results are summarized in Table 3, from which we see that the metaheuristic solutions again produce significantly improved objective values over the simple signal strategies. In particular, PSO reduces the network-wide total travel cost by 25.1% over 'Equal' and 43.4% over 'Capacity'. Figure 17 shows, within the best solution, the time-varying green splits allocated to link 6 and 22 in the network.

Algorithm	Best obj.	Worst obj.	Aver. obj.	CPU time (s)
SA	1.1283e+04	1.3117e+04	1.2161e+04	4101
NP	1.5472e+04	1.6577e+04	1.6121e+04	13989
PSO	1.0688e+04	1.1980e+04	1.1251e+04	7159
Equal	1.4992e+04	1.4992e+04	1.4992e+04	—
Capacity	1.9818e+04	1.9818e+04	1.9818e+04	—

Table 3: Optimization results for the Sioux Falls network.

Summarizing the test results on the two networks, we conclude that PSO provides the best solution quality measured by best, worst, and average objective values. However, this is offset by the higher computational times compared to SA. SA is the fastest algorithm among the three, although its solution quality is slightly worse than PSO. NP is outperformed by both PSO and SA in terms of solution quality and computational efficiency.

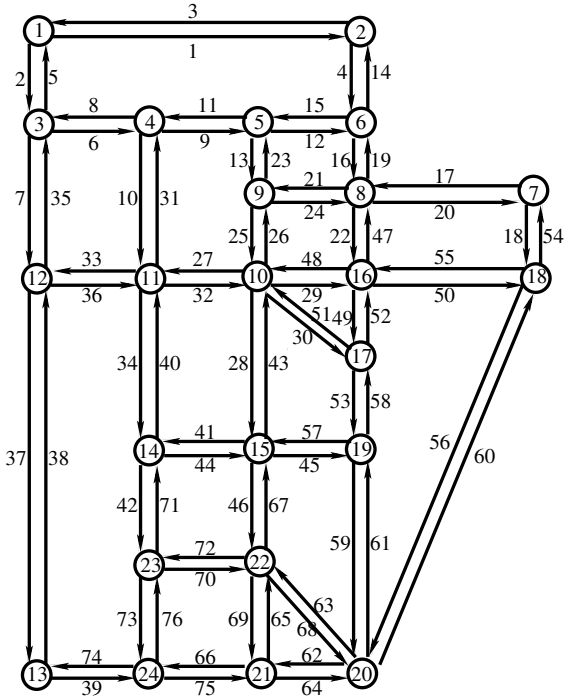

Figure 16: The Sioux Falls network.

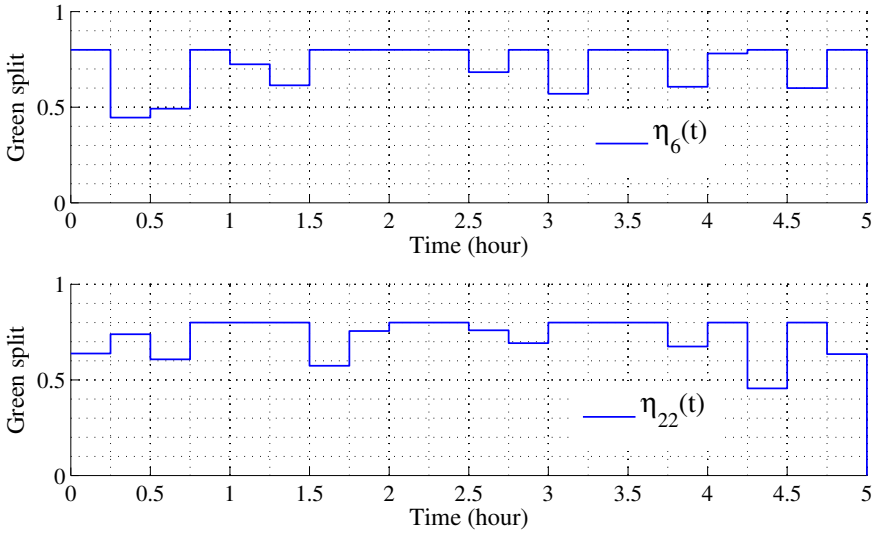

Figure 17: Sioux Falls network: The best solution for $\eta_6(t)$ and $\eta_{22}(t)$ obtained from PSO.

5.4. Algorithm acceleration via parallel computing

To improve the computational efficiency of PSO while maintaining its effectiveness in finding a satisfactory solution, we implement a parallelization of the PSO algorithm on 4 computing nodes for both test networks. The results are presented in Table 4, from which we can see 61.05% and 66.58% improvements in the computational efficiency for the seven-arc network and the Sioux Falls network respectively. Furthermore, based on 10 replications of the parallel computing procedure, we calculate the p-value for the objective values to determine the difference between the solu-

tion quality of sequential and parallel PSOs. And the p-values of 0.907 (seven-arc network) and 0.810 (Sioux Falls network) imply that the differences are insignificant. We thus conclude that the parallel implementation of the PSO algorithm may significantly accelerate the solution procedure without significantly deteriorating the solution quality.

Network	Seven-arc network		Sioux Falls network	
Algorithm	CPU time (s)	p-vallue	CPU time (s)	p-vallue
Sequential PSO	2154	0.907	7250	0.810
Parallel PSO	839	—	2423	—

Table 4: Comparison between the sequential and parallel PSO.

6. Conclusion and future research

This paper presents a bi-level Stackelberg game approach for optimizing signal timings on a network, based the continuum signal representation to describe and predict the aggregate traffic dynamics at signalized intersections. The proposed problem is capable of capturing drivers' adaptive travel decisions in response to the implemented signal timing plans. The upper-level problem seeks to minimize network-wide travel costs by controlling time-varying signal green splits at road intersections; the lower-level problem is a dynamic user equilibrium (DUE) with embedded LWR-based dynamic network loading (DNL) sub-model that employs the continuum signal approximation instead of the traditional binary (on-and-off) representation. Implementation details of the continuum signal model in the DNL procedure are provided based on the discussion from Han et al. (2014). The bi-level signal optimization problem is formulated as a mathematical program with equilibrium constraints (MPEC) and solved with three metaheuristic methods. Solution quality, computational efficiency, and parameter sensitivity of these methods are analyzed and compared. A parallelization of one of the methods is presented and its acceleration on the solution procedure is illustrated.

One of the novel aspects of the proposed model is the use of a continuum signal model, which is an effective alternative to the more conventional and exact on-and-off signal model. The continuum signal model has the ability to predict the aggregate traffic behavior that exists at signalized intersections without knowledge of detailed signal phasing, vehicle movement, and vehicle queuing/discharging. For this reason, it is suitable for applications on large-scale urban networks with considerable advantages in computational efficiency. Compared with the on-and-off approach, the continuum model does not rely on the binary (i.e. on-and-off) signal controls, allows larger time step sizes to be employed for improved computational efficiency, yields much more refined decision resolution in terms of green splits, and eliminates undesirable travel time discontinuities that typically arise when on-and-off signal models are considered. Despite these advantages, the effectiveness of the continuum model as an approximation of the on-and-off model is dependent on several factors including spillback and the fundamental diagram (Han et al., 2014). And the continuum signal model may yield significant error compared with the exact on-and-off approach if not properly implemented. We provide some practical guidance regarding the use of the continuum signal model to improve its approximation efficacy.

The proposed MPEC is computationally challenging due to the nonconvexity and semi-infiniteness of the equilibrium constraint, as well as the poor regularity in the constraints/objectives caused by the LWR-based DNL sub-model. Three metaheuristics are proposed in order to strike a balance between the optimality of the solution and the efficiency of the solution procedure. One of the metaheuristics is implemented with parallelization with a significantly improved computational efficiency. The resulting solutions reveal interesting managerial insights such as a Braess-like paradox and complex decisions in terms of time-varying signal green splits. However, the signal control decisions do not include parameters such as cycle, offset, and signal phases. Further study is required to determine these additional signal control parameters through the maximization of intersection capacities and throughputs.

References

Abdelfatah, A.S., Mahmassani, H.S., 1998. System optimal time-dependent path assignment and signal timing in traffic network. Transportation Research Record: Journal of the Transportation Research Board 1645 (1), 185-193.

Abdelfatah, A.S., Mahmassani, H.S., 2011. A simulation-based signal optimization algorithm within a dynamic traffic assignment framework. In: Intelligent Transportation Systems Conference Proceedings, Oakland 428-433.

Al-Shihabi, S., Merz, P., Wolf, S., 2008. Nested partitioning for the minimum energy broadcast problem. Learning and Intelligent Optimization. Lecture Notes in Computer Science 5313, 1-11.

Allsop, R.E., 1974. Some possibilities for using traffic control to influence trip distribution and route choice. In: Proceedings of 6th International Symposium on Transportation and Traffic Theory.

Aubin, J.P., Bayen, A.M., Saint-Pierre, P., 2008. Dirichlet problems for some Hamilton-Jacobi equations with inequality constraints. SIAM Journal on Control and Optimization 47 (5), 2348-2380.

Banks, A., Vincent, J., Anyakoha, C., 2007. A review of particle swarm optimization. Part I: background and development. Natural Computing 6 (4), 467-484.

Bressan, A., 2000. *Hyperbolic Systems of Conservation Laws. The One Dimensional Cauchy Problem*. Oxford University Press.

Bressan, A., Han, K., 2011. Optima and equilibria for a model of traffic flow. SIAM Journal on Mathematical Analysis 43 (5), 2384-2417.

Bressan, A., Han, K., 2012. Nash equilibria for a model of traffic flow with several groups of drivers. ESAIM: Control, Optimization and Calculus of Variations 18 (4), 969-986.

Cantarella, G.E., Gennaro, I., Antonio, S., 1991. Iterative procedure for equilibrium network traffic signal setting. Transportation Research Part A: General 25 (5), 241-249.

Cantarella, G.E., Sforza, A., 1995. Network design models and methods for urban traffic management. Urban Traffic Networks. Springer Berlin Heidelberg 123-153.

Cao, Y.J., Ireson, N., Bull, L., Miles, R., 1999. Design of a traffic junction controller using classifier system and fuzzy logic. Computational Intelligence. Springer Berlin Heidelberg 342-353.

Černý, V., 1985. A thermodynamic approach to the traveling salesman problem: An efficient simulation. Journal of Optimization Theory and Applications 45, 41-51.

Chen, O.J., Ben-Akiva, M.E., 1998. Game-theoretic formulations of interaction between dynamic traffic control and dynamic traffic assignment. Transportation Research Record: Journal of the Transportation Research Board 1617 (1), 179-188.

Claudel, C.G., Bayen, A.M., 2010. Lax-Hopf based incorporation of internal boundary conditions into Hamilton-Jacobi equation. Part I: theory. IEEE Transactions on Automatic Control 55 (5), 1142-1157.

Dafermos, C.M., 1972. Polygonal approximations of solutions of the initial value problem for a conservation law. Journal of Mathematical Analysis and Applications 38 (1), 33-41.

Daganzo, C.F., 1994. The cell transmission model. Part I: A simple dynamic representation of highway traffic. Transportation Research Part B 28 (4), 269-287.

Daganzo, C.F., 1995. The cell transmission model. Part II: Network traffic. Transportation Research Part B 29 (2), 79-93.

Friesz, T.L., Tobin, R.L., Cho, H.-J., Mehta, N.J., 1990. Sensitivity analysis based heuristic algorithms for mathematical programs with variational inequality constraints. Mathematical Programming 48, 265-284.

Friesz, T.L., Bernstein, D., Smith, T., Tobin, R., Wie, B., 1993. A variational inequality formulation of the dynamic network user equilibrium problem. Operations Research 41 (1), 80-91.

Friesz T.L., Han, K., Neto, P.A., Meimand, A., Yao, T., 2013. Dynamic user equilibrium based on a hydrodynamic model. Transportation Research Part B 47 (1), 102-126.

Friesz, T.L., Kim, T., Kwon, C., Rigdon, M.A., 2011. Approximate network loading and dual-time-scale dynamic user equilibrium. Transportation Research Part B 45 (1), 176-207.

Friesz, T.L., Mookherjee, R., 2006. Solving the dynamic network user equilibrium with state-dependent time shifts. Transportation Research Part B 40 (3), 207-229.

Gartner, N.H., Chronis S., 1998. Integration of dynamic traffic assignment with real-time traffic adaptive control system. Transportation Research Record: Journal of the Transportation Research Board 1644 (1), 150-156.

Gayah, V.V., Daganzo, C.F., 2012. Analytical capacity comparison of one-way and two-way signalized street networks. Transportation Research Record 2301, 76-85.

Ge, Y.E., Zhou, X., 2012. An alternative definition of dynamic user optimum on signalised road networks. Journal of Advanced Transportation 46 (3), 236-253.

Guler, S.I., Cassidy, M.J., 2012. Strategies for sharing bottleneck capacity among buses and cars. Transportation Research Part B 46 (10), 1334-1345.

Han, K., 2013. An analytical approach to sustainable transportation network design. Ph.D. dissertation, Pennsylvania State University.

Han, K., Friesz, T.L., Yao, T., 2013a. A partial differential equation formulation of Vickrey's bottleneck model, part I: Methodology and theoretical analysis. Transportation Research Part B 49, 55-74.

Han, K., Friesz, T.L., Yao, T., 2013b. A partial differential equation formulation of Vickrey's bottleneck model, part II: Numerical analysis and computation. Transportation Research Part B 49, 75-93.

Han, K., Szeto, W.Y., Friesz, T.L., 2014. Formulation, existence, and computation of simultaneous route-and-departure choice bounded rationality dynamic user equilibrium with fixed or endogenous user tolerance. Preprint available at http://arxiv.org/abs/1402.1211

Han, K., Piccoli, B., Gayah, V., Friesz, T.L., Yao, T., 2014. On the continuum approximation of the on-and-off signal control on dynamic traffic networks. Transportation Research Part B 61, 73-97.

Han, L., Ukkusuri, S., Doan, K., 2011. Complementarily formulations for the cell transmission model based dynamic user equilibrium with departure time choice, elastic demand and user heterogeneity. Transportation Research Part B 45 (10), 1749-1767.

Improta, G., Cantarella, G. E., 1984. Control system design for an individual signalized junction. Transportation Research Part B 18 (2), 147-167.

Karoonsoontawong, A., Waller, S.T., 2009. Application of Reactive Tabu Search for Combined Dynamic User Equilibrium and Traffic Signal Optimization Problem. Transportation Research Record: Journal of the Transportation Research Board 2090 (1), 29-41.

Kennedy, J., Eberhart, R., 1995. Particle swarm optimization. In Proceedings of IEEE International Conference on Neural Networks 4, 1942-1948.

Kirkpatrick, S., Gelatt, C.D., Vecchi, M.P., 1983. Optimization by simulated annealing. Science 200 (4598), 671-690.

Lebacque, J., Khoshyaran, M., 1999. Modeling vehicular traffic flow on networks using macroscopic models, in Finite Volumes for Complex Applications II, 551-558, Hermes Science Publications, Paris, 1999.

Lighthill, M., Whitham, G., 1955. On kinematic waves. II. A theory of traffic flow on long crowded roads. Proceedings of the Royal Society of London. Series A, Mathematical and Physical Sciences 229 (1178), 317-345.

Lin, Q., Kwan, B.W., Tung, L.J., 1997. Traffic signal control using fuzzy logic. In: Proceeding IEEE Systems, Man and Cybernetics, Orlando, FL 1644-1649.

Lo, H.K., 1999. A novel traffic signal control formulation. Transportation Research Part A 33 (6) 433-448.

Lo, H.K., 2011. A cell-based traffic control formulation: strategies and benefits of dynamic timing plans. Transportation Science 35 (2) 148-164.

Machemehl, R.B., Lee, C., 2005. Combined traffic signal control and traffic assignment: algorithms, implementation and numerical results. No. SWUTC/05/472840-00074-1.

Meneguzzer, C., 1995. An equilibrium route choice model with explicit treatment of the effect of intersections. Transportation Research Part B 29 (5), 329-356.

Merchant, D.K., Nemhauser, G.L., 1978a. A model and an algorithm for the dynamic traffic assignment problem. Transportation Science 12 (3), 183-199.

Merchant, D.K., Nemhauser, G.L., 1978b. Optimality conditions for a dynamic traffic assignment model. Transportation Science 12 (3), 200-207.

Miller, A.J., 1963. Computer control system for traffic networks. Proceedings of the 2nd International Symposium on Theory of Traffic Flow, London, UK.

Moskowitz, K., 1965. Discussion of 'freeway level of service as influenced by volume and capacity characteristics' by D.R. Drew and C.J. Keese. Highway Research Record 99, 43-44.

Mounce, R., 2006. Convergence in a continuous dynamic queuing model for traffic networks. Transportation Research Part B 40 (9), 779-791.

Pang, J., Han, L., Ramadurai, G., Ukkusuri, S., 2011. A continuous-time linear complementarity system for dynamic user equilibria in single bottleneck traffic flows. Mathematical Programming, Series A 133 (1-2), 437-460.

Papageorgiou, M., Blosseville, J., Hadj-Salem, H., 1990. Modelling and realtime control of traffic flow on the southern part of boulevard peripherique in paris: Part i: Modelling. Transportation Research Part A: General 24(5), 345 - 359, 1990.

Richards, P.I., 1956. Shockwaves on the highway. Operations Research 4 (1), 42-51.

Robertson, D.J., Bretherton, R.D., 1974. Optimal control of an intersection for any known sequences of vehicle arrivals. Proceedings of the 2nd IFAC-IFIP-IFORS Sumposium on Traffic Control and Transport Systems, Monte Carlo.

Savsani, V., Rao, R., Vakharia, D.P., 2010. Optimal weight design of a gear train using particle swarm optimization and simulated annealing algorithms. Mechanism and Machine Theory 45 (3), 531-541

Sha, D., Hsu, C.-Y., 2007. A new particle swarm optimization for the open shop scheduling problem. Computers & Operations Research 35 (10), 3243-3261.

Shelby, S., 2004. Single-intersection evaluation of real-time adaptive traffic signal control algorithms. Transportation Research Record 1867, 183-192.

Shi, Y., Liu, H., Gao, L., Zhang, G., 2011. Cellular particle swarm optimization. Information Sciences 181 (20), 4460-4493.

Shi, L., Ólafsson, S., 2000a. Nested partitions method for global optimization. Operations Research 48 (3), 390-407.

Shi, L., Ólafsson, S., 2000b. Nested partitions method for stochastic optimization. Methodology and Computing in Applied Probability 2 (3), 271-291.

Smith, M.J., Wisten, M.B., 1994. Lyapunov methods for dynamic equilibrium traffic assignment. In Proceedings of the Second Meeting of the EURO Working Group on Urban Traffic and Transportations, 223-245, INRETS, Paris.

Smith, M.J., Wisten, M.B., 1995. A continuous day-to-day traffic assignment model and the existence of a continuous dynamic user equilibrium. Annals of Operations Research 60 (1), 59-79.

Sun, D., Benekohal, R.F., Waller, S.T., 2006. Bi-level Programming Formulation and Heuristic Solution Approach for Dynamic Traffic Signal Optimization. Computer-Aided Civil and Infrastructure Engineering 21 (5), 321-333.

Szeto, W.Y., Lo, H.K., 2006. Dynamic traffic assignment: Properties and extensions. Transportmetrica 2 (1), 31-52.

Ukkusuri, S., Doan, K., Aziz, H.M., 2013. A bi-level formulation for the combined dynamic equilibrium based traffic signal control. Procedia-Social and Behavioral Sciences 80, 729-752.

Vickrey, W.S., 1969. Congestion theory and transport investment. The American Economic Review 59 (2), 251-261.

Wie, B.W., Tobin R.L., Carey. M., 2002. The existence, uniqueness and computation of an arc-based dynamic network user equilibrium formulation. Transportation Research Part B 36, 897-918.

Yang, H., Yagar, S., 1995. Traffic assignment and signal control in saturated road networks. Transportation Research Part A: Policy and Practice 29 (2) 125-139.

Yin, P., 2006. Particle swarm optimization for point pattern matching. Journal of Visual Communication & Image Representation 17, 143-162.

Yperman, I., Logghe, S., Immers, L., 2005. The link transmission model: an efficient implementation of the kinematic wave theory in traffic networks, Advanced OR and AI Methods in Transportation. In Proceedings of 10th EWGT Meeting and 16th Mini-EURO Conference, Poznan, Poland, 122-127, Publishing House of Poznan University of Technology.